

Development of a Model for Predicting the Knock Boundary in Consideration of Cooled Exhaust Gas Recirculation at Full Load

Alexander Fandakov¹(✉), Michael Grill⁵, Michael Bargende¹, Max Mally², Marco Günther², Stefan Pischinger², Liming Cai³, Heinz Pitsch³, Karl Alexander Heufer⁴, Ajoy Ramalingam⁴, Heiko Minwegen⁴, and André Casal Kulzer⁶

¹ Institute of Internal Combustion Engines and Automotive Engineering, University of Stuttgart, Stuttgart, Germany

alexander.fandakov@ivk.uni-stuttgart.de

² Institute for Combustion Engines, RWTH Aachen University, Aachen, Germany

³ Institute for Technical Combustion, RWTH Aachen University, Aachen, Germany

⁴ Physico-Chemical Fundamentals of Combustion, RWTH Aachen University, Aachen, Germany

⁵ FKFS – Research Institute of Automotive Engineering and Vehicle Engines Stuttgart, Stuttgart, Germany

⁶ Porsche AG, Weissach, Germany

Abstract. Engine knock limits the efficiency of turbocharged SI engines at high loads. The occurrence of this phenomenon can be inhibited by deploying recirculation of cooled exhaust gas (EGR) at full load. However, the development of full load EGR combustion systems cannot be performed in the 0D/1D engine simulation, as no meaningful models for the reliable prediction of the knock limit under the influence of EGR exist.

Measurements of ignition delay times in a shock tube and a rapid compression machine under the influence of exhaust gas have been carried out. The addition of 25% EGR prolonged the ignition delay time up to 100%. A detailed reaction mechanism for gasoline surrogates was defined and validated against the measurement results. Furthermore, the effects of EGR on combustion, knock behavior and emissions were investigated on a single-cylinder re-search engine. The center of combustion could be advanced by up to 9° CA with the addition of EGR leading to a four percent higher indicated efficiency. The influence of catalytically treated exhaust gas was examined as well. At high EGR rates of 25% catalytically treated exhaust gas allowed a 2° CA earlier center of combustion. Furthermore, the influence of nitric oxide on the knocking tendency was investigated. It has been found that a total cylinder NO concentration of about 100 ppm leads to the highest knocking tendency. At NO concentrations below 40 ppm NO the knocking tendency was decreased. Higher concentration than 100 ppm of NO in the cylinder decreased knocking tendency as well.

The pressure trace analysis of the measured single working cycles shows that the pre-reaction state of the unburned mixture at knock onset calculated with commonly used knock models decreases with rising EGR rate and engine speed, although by definition it must be constant at the time of auto-ignition. Consequently, reaction kinetics simulations at in-cylinder conditions proved that, under specific boundary conditions, the auto-ignition of the unburnt mixture resulting in knock happens in two stages. In this case, low-temperature ignition occurs in the unburnt mixture while the combustion is taking place. This phenomenon significantly influences the ignition delay of the mixture, which severely impairs the prediction capabilities of commonly used knock models.

Based on these findings, a new knock modeling approach capable of predicting the low-temperature ignition occurrence as well as reproducing its influence on the mixture's auto-ignition was developed. The results from 3D-CFD simulations accompanying the model development supported all model assumptions made. The developed knock model was successfully validated against measurement data at various boundary conditions, such as different inlet temperatures and mixture compositions as well as EGR rate and engine speed variations. It can predict the knock limit very accurately with errors in center of combustion below 2° CA and thus contributes to an efficient development process of full load EGR combustion systems in the 0D/1D engine simulation.

1 Introduction

The knock limitation at higher loads is one of the major challenges for increasing the efficiency of gasoline engines. For low part load fuel consumption a high compression ratio is desirable but a compromise with full load efficiency must be made. Another challenge is the component protection at higher engine loads and speeds due to exhaust gas temperature limitations. Currently enrichment is used but the upcoming "Real Driving Emissions" legislation will not permit this strategy anymore. A suitable countermeasure is the application of high load exhaust gas recirculation to overcome both challenges.

Yet, the development of a high load EGR combustion system is complex. The engine needs a specific layout of the charging system, the charge air and EGR cooling system and various other parameters, like compression ratio and valve timing. Due to the complexity of the layout phase only 0D/1D engine simulation can be applied. Thanks to the high prediction quality of the models and the low computational times, this is a powerful tool used to reduce development costs by partially eliminating the need for cost-intensive test bench investigations. However, the existing models for predicting knocking combustion in 0D/1D SI engine simulations are known for their poor performance and the great effort needed for their calibration. Hence, the reliable prediction of knock occurrence is a challenging task, especially if the entire engine map has to be considered. This fact results in significant restrictions on the development of full load EGR combustion systems with the help of 0D/1D simulations. Therefore, except the fundamental understanding of the effects of EGR, the goal of this work is the development of a reliable knock model for the application in EGR combustion system development.

2 Fundamental Combustion Kinetic Investigation

The development of the chemical kinetic mechanism for the combustion of gasoline fuels and their surrogates is described in this section. Due to the limited ignition delay time data for model validation, especially at low temperature conditions with EGR, fundamental kinetic measurements of ignition delay times were performed in a rapid compression machine and a shock tube for an ethanol-doped research grade gasoline (RON95E10). The obtained data covers a wide range of conditions including initial temperatures, equivalence ratios, pressures, and EGR ratios. The model was derived based on the state-of-the-art kinetic knowledge as well as advanced mathematical methods and was validated successfully against the data obtained as part of this study and those available in the literature.

2.1 Experimental Investigation

Rapid compression machine

The ignition delay times in the low-to-intermediate temperature regimes were measured in a rapid compression machine (RCM). A complete description of the facility can be found in Ref. [Lee12]. Briefly, the reaction chamber of the RCM, the mixing vessels along with the tubing's are electrically heated in order to accommodate the high boiling components of the provided gasoline. The initial temperature is monitored by type 'T' thermocouples mounted on the reaction chamber. The mixtures were prepared with the aid of two static pressure sensors which monitor the partial pressures required for the mixtures. The dynamic pressure changes during a reactive experiment were recorded with the help of PCB 113B24 sensor. The Kistler 6125C pressure sensor was used during a non-reactive experiment in order to account for the thermal heat shock resistance. The compressed temperature was calculated using the adiabatic compression and expansion routine of Gaseq [Mor05]. The experimental uncertainty on compressed temperature using error propagation analysis was estimated to be ± 5 K and the observed variation in ignition delay time is within 10%. In the RCM, heat loss and radical pool generation during compression phase are the two non-idealities that affect the reactivity behavior at longer and shorter ignition delay times, respectively, and it is essential to include these effects during the zero-dimensional simulations by using non-reactive pressure profiles [Sun14].

Shock tube

The ignition delay times in the high temperature regime were measured in a shock tube (ST) facility. Its detailed description is available in Ref. [Zha16]. The complete driven section of the ST, mixing vessel, and the connecting tubes are electrically heated and monitored by type 'T' thermocouples. The partial pressures of the mixture preparation process were monitored with two static pressure sensors. The dynamic pressure changes in the driven section of the ST were recorded with 5 PCB 113B22 pressure sensors which are used for the determination of shock velocity. The reflected shock conditions were calculated using an in-house code based on the shock and detonation toolbox [She14] routines implemented for Cantera [Goo15]. The uncertainty in the

reflected shock temperature and pressure is estimated to be 1.1% and 3.5%, respectively, while that of the ignition delay time is 20%. At longer ignition delay times, the effect of boundary layers constitutes to a constant rate of pressure rise, thereby affecting the reactivity behavior. This non-ideal behavior can be included during the simulations by assuming an average pressure rise of 8%/ms.

Measurement of ignition delay times

The ignition delay times for a fully characterized research grade gasoline (RON95E10) were measured at the conditions defined in Table 1. The composition of exhaust gas was specified with respect to lean and rich conditions. As mentioned above, the experimental work aids in providing a comprehensive data set for the validation of chemical models.

Table 1. Measurement of ignition delay times in the RCM and ST

Pressure/bar	Rel. AFR/1	EGR rate/%	Exhaust gas composition/mass %				
			N ₂	CO ₂	CO	H ₂ O	H ₂
20–40	0.85	0	–	–	–	–	–
20–40	1.30	0	–	–	–	–	–
20–40	0.85	25	71.21	14.15	5.16	9.35	0.11
20–40	1.30	25	72.29	18.87	–	8.83	–

2.2 Fuel Properties and Surrogate Formulation

The gasoline, RON95E10, was supplied by Shell global solutions GmbH. Its key properties are summarized in Table 2. In addition, its temperature-dependent specific heats and distillation curve were also characterized for the calculation of compressed

Table 2. Properties of RON95E10 and the proposed surrogate mixture.

Property	RON95E10	Surrogate ^a	Surrogate ^b	Surrogate ^c
RON/-	96.5	95.0	91.3	96.2
MON/-	85.2	86.6	87.2	88.7
RON-MON/-	11.3	8.4	4.1	7.5
H/C ratio/-	1.94	1.93	1.93	
Density/kg/l	0.7417	0.7443	0.7443	0.7493
Composition/mass%	10.3% Ethanol	13.6% n-Heptane 45.7% iso-Octane 30.5% Toluene 10.3% Ethanol		

^aRON and MON are calculated using the proposed blending rules.

^bRON and MON are determined based on the volumetric-blending rule.

^cProperties are measured.

mixture temperatures in RCM measurements and for the specification of initial temperatures in the reactor and mixing vessel, respectively.

Since real petroleum fuels are composed of a large variety of hydrocarbon components, surrogate mixtures of only few representative species are typically employed in computational research and in engine development. For ethanol-doped gasoline fuels, mixtures of n-heptane, iso-octane, toluene, and ethanol are commonly used as the surrogate components and their composition is optimized to mimic target properties of real fuels. In general, the properties, research octane number (RON), motor octane number (MON), H/C ratio, and liquid density, are of interest due to their importance. To calculate the H/C ratio and liquid density of surrogate mixtures, mole- and volume fraction-based blending rules are used, respectively. For the determination of RON and MON, volumetric blending approach is applied in general. However, recent studies [Mor10,And10] reveal that this approach reproduces the RON and MON of surrogate fuels with large uncertainties. Therefore, a revised blending rule for RON and MON of ethanol-doped gasolines is proposed here. For the base gasoline fuel, which is emulated with the mixtures of n-heptane, iso-octane, and toluene, non-linear volumetric blending approach [Mor10] is applied to determine their octane numbers. Mole fraction-based blending rule is then employed to determine the RON and MON for the mixtures of the base gasoline fuel and ethanol, following the suggestion of Andersen et al. [And10]. The MON and RON can be calculated as follows:

$$\begin{aligned}
 RON = (1 - X_{Eth}) & \left(100 \frac{X_{Iso}}{X_{Iso} + X_{Hep}} + \right. \\
 & 142.79 \frac{X_{Tol}}{X_{Iso} + X_{Hep} + X_{Tol}} - 22.65 \left(\frac{X_{Tol}}{X_{Iso} + X_{Hep} + X_{Tol}} \right)^2 \\
 & \left. - 111.95 \frac{X_{Iso}}{X_{Iso} + X_{Hep}} \frac{X_{Tol}}{X_{Iso} + X_{Hep} + X_{Tol}} \right) + X_{Eth} RON_{Eth}
 \end{aligned} \quad (1)$$

$$\begin{aligned}
 MON = (1 - X_{Eth}) & \left(100 \frac{X_{Iso}}{X_{Iso} + X_{Hep}} + \right. \\
 & 128 \frac{X_{Tol}}{X_{Iso} + X_{Hep} + X_{Tol}} - 19.21 \left(\frac{X_{Tol}}{X_{Iso} + X_{Hep} + X_{Tol}} \right)^2 \\
 & \left. - 119.24 \frac{X_{Iso}}{X_{Iso} + X_{Hep}} \frac{X_{Tol}}{X_{Iso} + X_{Hep} + X_{Tol}} \right) + X_{Eth} MON_{Eth}
 \end{aligned} \quad (2)$$

with X_{Iso} , X_{Hep} , X_{Tol} , and X_{Eth} indicating the mole fraction of iso-octane, n-heptane, toluene and ethanol in the surrogate mixtures, respectively. RON_{Eth} and MON_{Eth} are the octane numbers of ethanol.

The surrogate composition is optimized numerically by minimizing the property differences between real and surrogate fuels. The compositions and the calculated surrogate properties are presented in Table 2, in comparison with those of the RON95E10. As the validation of the suggested blending rule, the key properties of the proposed surrogates were measured and shown in Table 2, together with the RON and MON calculated with the conventional volumetric-blending rules. It can be seen that application of the revised blending rules leads to improved prediction accuracy of the RON and octane sensitivity (RON-MON).

2.3 Development of a Kinetic Mechanism for Gasoline Surrogate Fuels

The chemical mechanism was developed based on the published mechanism for gasoline surrogate fuels from Cai et al. [Cai16]. The reference mechanism [Cai16] includes the oxidation chemistry of various C₀–C₈ hydrocarbon species and substituted aromatic species, including n-heptane, iso-octane, toluene, and ethanol, allowing the formulation of multi-component surrogate fuels with capability of predicting Polycyclic Aromatic Hydrocarbon (PAH) formation in gasoline engines. Recent studies [Cai16_2] suggested the modification of oxidation chemistry of alkanes in terms of thermochemistry, reaction rates, and pathways. The aim is to avoid the error compensation in chemical models and to improve the model prediction ability of ignition delay times, which is of particular importance in this work for the prediction of knocking behavior. Therefore, the sub-models for n-heptane and iso-octane in the reference mechanism [Cai16] are revised according to the state-of-art kinetic knowledge.

The combustion chemistry of n-heptane was extracted from the recently published mechanism [Cai16_2] of normal alkanes, which includes the latest combustion kinetic knowledge in terms of thermochemistry, rate rules, and reaction pathways. Following the model development concept introduced in Ref. [Cai16_2], a revised iso-octane mechanism was proposed. The detailed mechanism for iso-octane from Curran et al. [Cur02] was first updated by incorporating recalculated thermochemical data of species involved in the oxidation of iso-octane using the group additivity method [Ben76] with the revised group values [Bur15]. Subsequently, the alternative reaction pathways of peroxy hydroperoxide species were included in the mechanism. Following this, the rate rules for the primary and secondary carbon sites were updated by using the rate rules recommended in Ref. [Cai16_2]. The rate rules for the tertiary sites were calibrated for good model performance using an uncertainty quantification framework [Cai16_2]. In order to reduce the computational cost, the detailed mechanisms for n-heptane and iso-octane were reduced to a skeletal level using a multi-stage reduction strategy developed by Pepiot-Desjardins and Pitsch [Pep07]. The reduced models were further built as additional modules upon the reference model [Cai16]. The mechanism consists of 489 chemical species and 3369 elementary reactions.

2.4 Model Validation

The measured ignition delay times of RON95E10 are shown in Fig. 1., compared to those calculated. Note that, facility effects of both setups are taken into account in the simulation. By means of the RCM and ST, the measured ignition data covers a very wide range of initial temperature, extending the validation database available in the literature. Reasonable agreement is observed between data and simulation results. More importantly, the model reflects the influence of pressure, equivalence ratio and EGR ratio very well, as illustrated in Fig. 2. The model was also validated successfully against the data available in the literature, such as ignition delay times and burning velocities. For the sake of brevity, these cases are not shown here.

This model will be coupled with 3D-CFD simulations in the following to study the knock behavior of gasoline with EGR at full load operating conditions reduction.

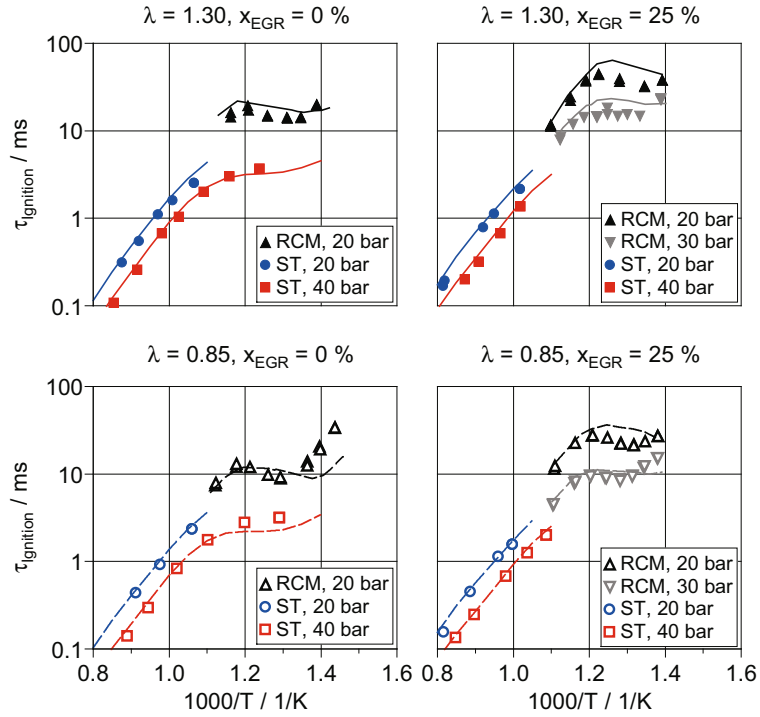


Fig. 1. Ignition delay times of RON95E10. Symbols and lines denote the data and the numerical results, respectively.

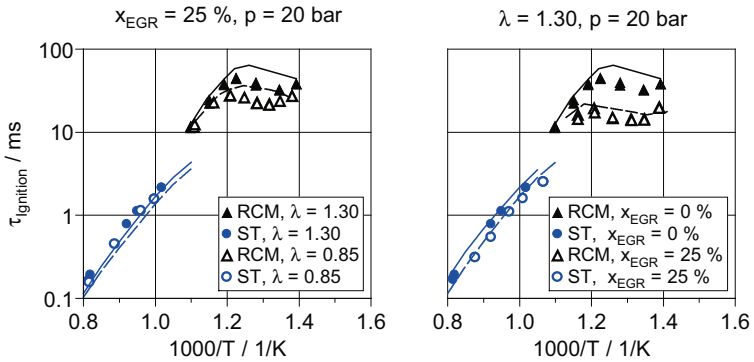


Fig. 2. Ignition delay times of RON95E10. Symbols and lines denote the data and the numerical results, respectively.

In order to reduce the CFD computational effort, a reduced model with 327 species and 1730 reactions was derived using the method of isomer lumping introduced in Ref. [Pep07]. Marginal difference (<1%) is observed between the reduced model and the detailed one with 428 species at conditions of interest.

3 Thermodynamic Testing

3.1 Experimental Setup

The experimental investigations were performed on a homogeneously operated direct injection spark ignition single cylinder research engine. The engine features external boosting, low pressure exhaust gas recirculation and a tumble generation device. The tumble generation device has been used at 50% actuation during the experimental investigations. Information about the level of charge motion and the flow performance can be found in [Jak11]. Further technical data of the engine is summarized in Table 3.

The layout of the cylinder head and combustion chamber dome is shown in Fig. 3. The engine features a central injector, which is located between the intake valves. A spark plug with a heat value of 8 according to NGK is mounted between the exhaust valves.

In order to perform testing under realistic boundary conditions the engine is equipped with an exhaust throttle to simulate the back pressure of the turbine. During boosted operation the average exhaust back pressure is controlled to be equal to the intake pressure. The extraction point of the low pressure EGR system is downstream of the throttle. The EGR inlet is located upstream of the external charging system (three-stage roots blower). In order to avoid condensation of water in the EGR cooler and the intake system the outlet temperature of the EGR cooler was set to 70 °C.

Table 3. Engine specifications

Engine specifications					
Stroke (s)	90.5	mm	Valve train	DOHC (4 V)	
Bore (D)	75	mm	Exhaust valve opening*	13 (bBDC)	° CA
s/D	1.207	1	Exhaust valve closing*	10 (bTDC)	° CA
Engine displacement	399	cm ³	Intake valve opening*	15 (aTDC)	° CA
Connection rod length	152	mm	Intake valve closing*	30 (aBDC)	° CA
Piston-pin offset (thrust side)	0.5	mm	Injection system	Bosch HDEV 5.2 DI solenoid multi-hole	
Compression ratio	10.9	1	Fuel pressure	200	bar

*: Referred to 1 mm lift

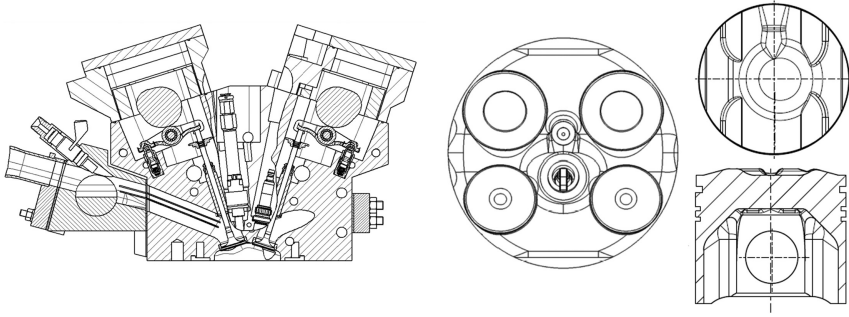


Fig. 3. Research engine layout: (a) Sectional view of cylinder head, (b) combustion chamber dome and (c) piston geometry for compression ratio of 10.9

The EGR rate is measured via CO_2 measurement in the exhaust and the intake system. Based on the measured concentrations the EGR rate can be calculated:

$$x_{\text{EGR}} = \frac{1}{1 + \frac{Y_{\text{CO}_2, \text{Exh}} - Y_{\text{CO}_2, \text{Int}}}{Y_{\text{CO}_2, \text{Int}} - Y_{\text{CO}_2, \text{Air}}} \cdot \frac{\dot{m}_{\text{Exh}}}{\dot{m}_{\text{Air}}} \cdot \frac{M_{\text{Air}}}{M_{\text{Exh}}}} \quad (3)$$

The exhaust gas composition was measured via a flame ionization detector (HC), a paramagnetic oxygen analyzer (O_2), an infrared gas analyzer (CO and CO_2), a chemiluminescence analyzer (NO_x) and a TSI EEPSTM (PN). Furthermore, the engine has been equipped with a conventional catalyst from a gasoline passenger car in order to run the engine with catalyzed exhaust gas. Due to the high volume of the catalyst and thus low space velocities a high conversion rate could be achieved. During catalyst operation the components in the exhaust gas were measured upstream and downstream of the catalyst. To investigate the influence of single reactive components of EGR on the combustion an external dosing system has been added prior to the charging system. High accuracy mass flow controllers were used to dose the single components into the intake system.

For all measurement points spark sweeps in the area of the knock limited spark advance have been carried out. The characteristic number of knocking combustion was set to be the knocking peak to peak (KPP) value of the high-pass filtered pressure trace. The limit for KPP was defined as engine speed divided by 1000 in bar. Since knocking is a statistic phenomenon the knock frequency is the criterion which has been used to define the knock limited spark advance (KLSA). If 3–10% of the cycles reveal a knocking combustion, it is defined that the engine is operating at the knock limit (the spark timing closest to 3% is chosen). Based on KLSA a spark timing sweep from 1° CA retarded to 1° CA advanced spark timing was conducted. Thus the measurement data contains operating points from slight to severe knock occurrence.

An overview of the test matrix is given in Table 4. Overview of experimental test matrix ($p_{\text{mi}} = 16$ bar). Measurements with rich and lean exhaust gas recirculation as well as the addition of CO and H_2 to the fresh charge have been carried out as well, but are not included for the sake of brevity. The EGR rate has been increased by increments

Table 4. Overview of experimental test matrix ($p_{mi} = 16$ bar)

EGR type	EGR rate/%	$T_{Intake}/^{\circ}C$	Rel. AFR/1	Engine speed/1/min	Synthetic component
Bef. Cat.	0–25	35–55	1.0	1500	–
Bef. Cat.	0–25	35–55	1.0	2500	–
Bef. Cat.	0–20	45–65	1.0	4000	–
Aft. Cat.	0–25	35–45	1.0	1500	–
Aft. Cat.	0–20	35–45	1.0	1500	NO

of 5% and the intake temperature by increments of 10 °C. The load has been fixed at 16 bar indicated mean effective pressure (pmi).

For validation datasets with a different cylinder head (tumble runner design) and an increased compression ratio of 11.84 have been generated. Besides the standard camshaft, data with a Miller camshaft (230° CA event length) have been generated as well. The load ranges from 12 to 20 bar p_{mi} . Thus, the validation database covers a wide range of the engine operation map.

3.2 Experimental Results

During baseline testing the engine was operated with non-catalyzed exhaust gas. In order to cover a wide range of thermodynamic states the intake temperature, the engine speed and the EGR rate have been varied.

A summary of the baseline results with EGR is given in Fig. 4. Only measurements at the KLSA are depicted. EGR proved to inhibit knock at all investigated points when the intake temperature is kept on a constant level. With increased EGR rate the spark timing had to be advanced in order to compensate the longer heat delay and duration. In all cases the spark timing could be advanced in that way, that an earlier center of combustion could be achieved. Subsequently the engine efficiency was increased with EGR. Another contributor to the increased efficiency is the reduced heat loss to the cylinder wall. The effect of reduced temperatures during combustion can be seen as well in the decrease of NO emissions. Due to the lower flame temperatures and thus increased flame quenching the HC emissions are increased.

For knock model development, the identification of the knock limited spark advance is of major importance. To this end, spark timing sweeps in steps of 0.5° CA were conducted. The results at 1500 1/min are depicted in Fig. 5. For the investigated cases, the number of knocking cycles is slightly increasing with advanced spark timing at first. Starting at the point of about 5% knock frequency, the number of knocking cycles steeply rises, indicating that the number of knocking cycles is following an exponential trend. For the cases with EGR, no significant differences in this behavior can be observed. The maximum peak to peak amplitude of the pressure oscillation is below 8 bar for all cases, except for the EGR rate of 20%. The point closest to 3% knocking cycles has been chosen as the KLSA. Regarding the dependence of the knock tendency on the spark timing relative to KLSA it can be concluded that the addition of EGR does not have a high impact on the knocking behavior of the engine itself.

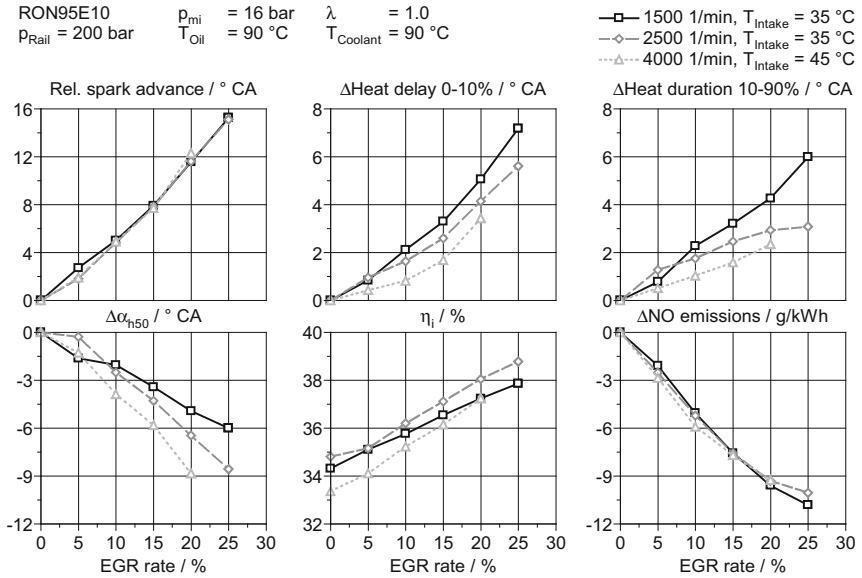


Fig. 4. Results of baseline investigation

The general trend in knock frequency was found for higher engine speeds as well. For 10% EGR, the comparison in dependence of the engine speed for knock frequency and maximum KPP are depicted in Fig. 6. The trend in knock frequency is very similar for all engine speeds. Nevertheless, the severity of the knock events is increasing with engine speed. At 2500 1/min an about 4.5 bar higher maximum KPP is observed compared to 1500 1/min. Taking the reduced duration of the pressure fluctuations at higher engine speeds into account, the stress due to the pressure fluctuations is similar for the points with the maximum KPP values.

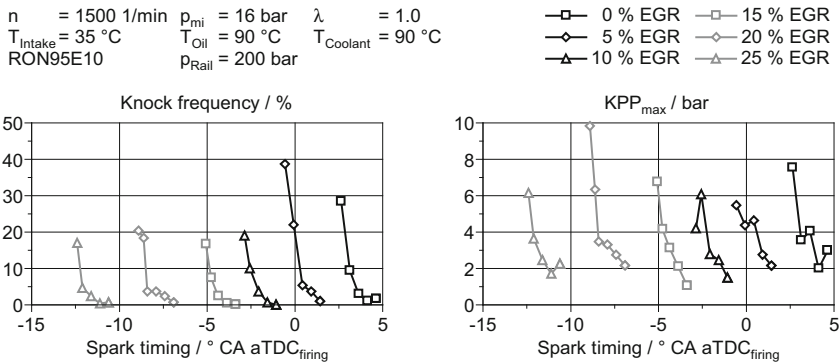


Fig. 5. Knock frequency and maximum KPP at 1500 1/min

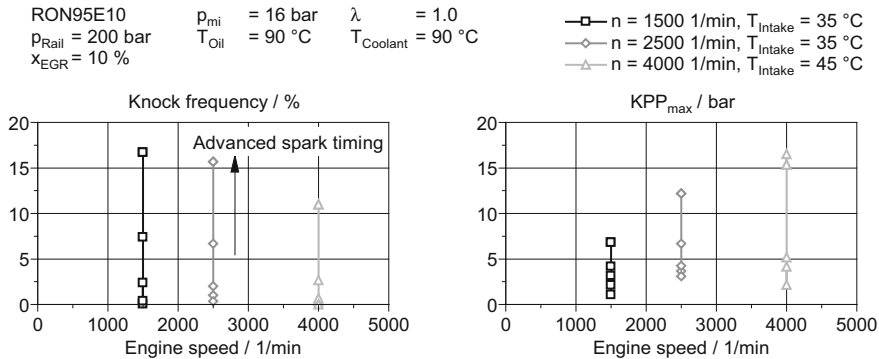


Fig. 6. Dependence of knock frequency and maximum KPP on engine speed

For the knock model development, spark timing sweeps at increased intake temperatures have been carried out as well. Thus, the measurement data covers a wide range of thermodynamic conditions in the end-gas, which allows the development of a reliable knock model for full load EGR combustion systems.

3.3 Investigation of the Influence of Nitric Oxide on Engine Knock

In dependency of the rel. AFR in the combustion chamber the exhaust gas composition is varying. About three-quarter of the volumetric composition is nitrogen, which does not have a strong chemical effect on the combustion. During rich combustion high amounts of CO and small amounts of H_2 are formed. For stoichiometric combustion higher concentrations of NO are formed. When the exhaust gas is recirculated these species can take part in the combustion process. For CO no influence on the auto-ignition in a HCCI engine was found [Deb06]. Hydrogen is known to increase the combustion speed and stability [Alg07]. Especially NO is considered to be a species which can strongly affect the auto-ignition in the cylinder. Various researches have investigated the influence of NO on knocking combustion but the results are often contradicting, as summarized in [Par15].

Measurements with NO addition to the intake charge were performed while running the engine with catalyzed exhaust gas. Due to the size of the catalyst the NO concentration could be reduced to less than 10 ppm in the recirculated exhaust gas. NO was added prior to the external boosting system in order to achieve a homogeneous mixing with the EGR and air. Measurements were performed with three different EGR rates and an intake NO concentration from 0 to 300 ppm (100 ppm steps). In order to take the cylinder NO concentration into account CFD simulations of the corresponding operating points were carried out to determine the internal residual gas mass fraction. With the exhaust gas measurement prior to the catalyst the internal NO concentration can be calculated. Finally, the total NO concentration is derived with the addition of external NO. With rising external EGR rate the internal NO rate is decreasing. The calculated NO concentration in the cylinder due to internal EGR is varying from 100 ppm at 0% EGR to 20 ppm at 20% EGR. The results are shown in Fig. 7.

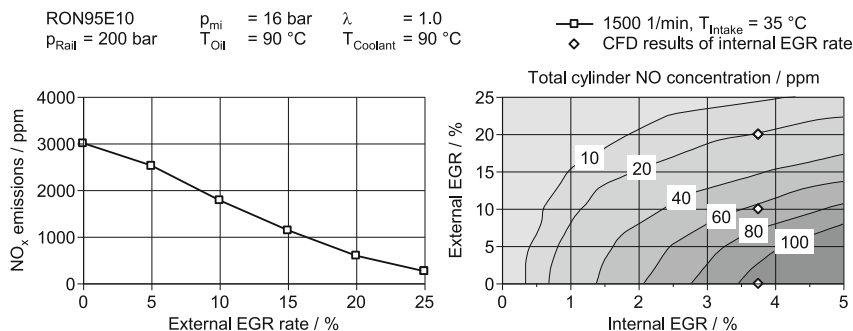


Fig. 7. Calculation of cylinder NO concentration based on pre-catalyst measurement and the internal EGR rate (calculated with CFD simulations)

The experimental results of the NO addition in the intake port are depicted in Fig. 8. The average combustion and the combustion stability are not affected by the addition of NO. However, the number of knocking cycles changes with the addition of NO. At 0% EGR the number of knocking cycles is reduced with the addition of NO. This gives an indication that the knock promoting effect of NO is already saturated at low NO concentrations in the cylinder. At 10% EGR no significant difference between 0 ppm and 100 ppm external NO is observed. With further increase of NO the number of knocking cycles decreases again. Surprisingly no knock promoting effect is observed at these two operating points. At 20% EGR the number of knocking cycles is drastically increasing at 100 ppm external NO. Again a further increase of external NO reduces the number of knocking cycles. This behavior was confirmed at a second intake temperature. Without knowledge of the internal EGR rate and the cylinder NO concentration this behavior cannot be explained. Taking the cylinder NO concentration into account it can be observed that the maximum knock promoting effect of NO is observed at about 100 ppm cylinder NO concentration. Higher NO concentrations as observed for the 0% EGR case lead to a reduced knock tendency. At 20% EGR the internal NO concentration is about 20 ppm NO. Here external addition of NO leads to a strong increase of knocking cycles. The effect is most pronounced at 100 ppm external NO. Further increase of cylinder NO concentration leads to a reduction of knocking cycles. These findings give a good indication about the different results obtained from literature. Often the internal residual gas mass fraction is unknown and thus the internal cylinder NO concentration cannot be derived from measurement results.

This phenomenon was further investigated with the detailed mechanism developed in Sect. 2.3. The underlying chemical reactions of the effect of NO on auto-ignition are shown in Fig. 9. On the one hand NO can promote auto-ignition at low temperatures via reaction with HO₂ which ultimately yields two OH radicals. At higher temperatures NO can react with OH radicals and form rather unreactive HONO. The second path ultimately leads to a chain termination. In Fig. 9 the effect of NO addition on ignition delay times is depicted. The auto-ignition delay time in the low temperature regime (here evaluated at 700 K) is decreased with addition of 100 ppm NO, but a further addition of NO does not have any effect. In the high temperature regime (evaluated

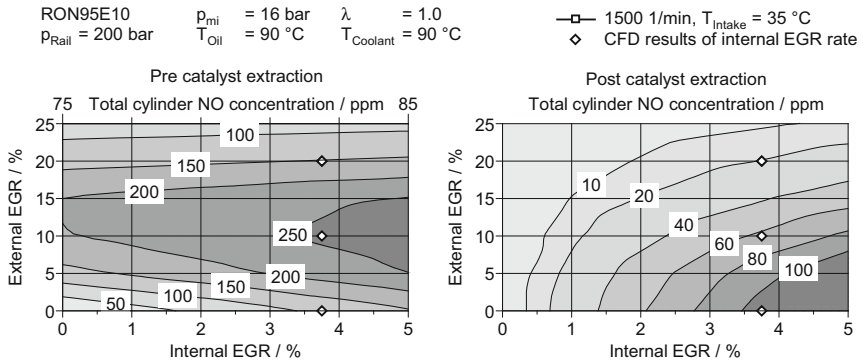


Fig. 10. Comparison of cylinder NO concentration between pre and post catalyst extraction

extraction the cylinder NO concentration cannot be reduced below 100 ppm for the investigated operating points. Peak concentration with pre catalyst extraction is slightly above 250 ppm. For post catalyst extraction the cylinder NO concentration can be decreased steadily with external EGR rate.

The experimental results for pre and post catalyst extraction at the KLSA are shown in Fig. 11. For low EGR rates no differences between pre and post catalyst extraction were apparent from the measurement data. First small differences appeared at 15% EGR rate which indicated a slightly less knock limitation for post catalyst extraction. With even higher EGR rates the spark timing could be further advanced with post catalyst extraction leading to a gain of about 2° CA in center of combustion. These findings are in-line with the measurement results of the single component investigation of NO. Similar trends were found at an inlet temperature of 45 °C.

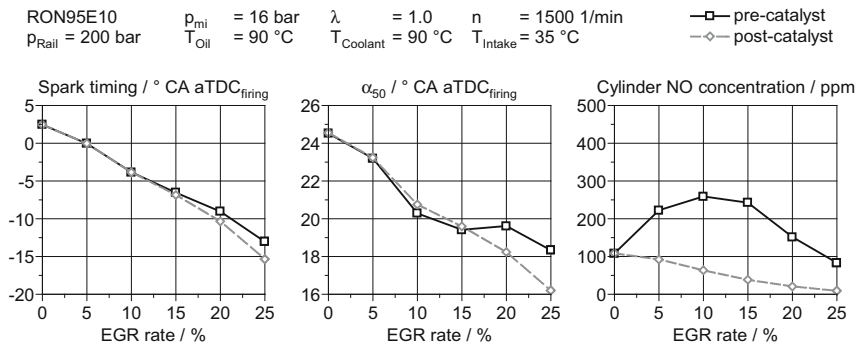


Fig. 11. Comparison of pre- and post-catalyst extraction

4 Numerical Investigation

For further understanding of the test bench results numerical investigations were carried out. The scope of the numerical investigation was to gain comprehension of the thermodynamic and mixture state in the cylinder during compression and combustion. Furthermore, the developed mechanism from Sect. 2.3 was coupled to the simulation model in order to simulate combustion and the occurrence of auto-ignition events. The numerical domain for the in-cylinder simulation includes the geometry of the single cylinder research engine from intake to exhaust pressure transducer. Crank angle resolved boundary conditions were used at the intake and exhaust boundary. The composition of the exhaust gas was calculated based on test bench measurements. Propane was used as chemical representative for HC emissions. The composition of the fresh charge was calculated as a perfect mixture of air and EGR depending on the operating points EGR rate. A comprehensive overview of the simulation model is given in Fig. 12.

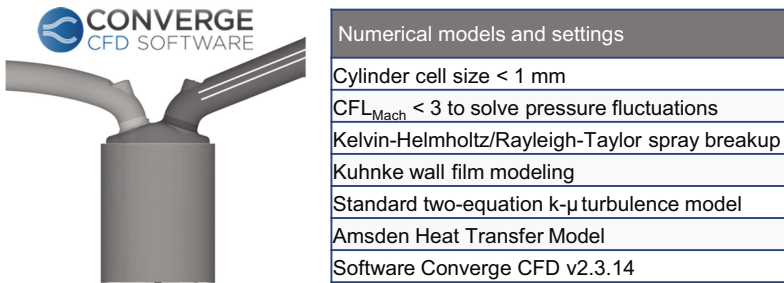


Fig. 12. Numerical models and settings for the in-cylinder 3D-CFD simulation

4.1 Analysis of Thermodynamic State

The thermodynamic and mixture state in the cylinder (temperature, pressure and composition) is the most important input parameter of the knock model. This state was assessed in detail with help of 3D-CFD simulations. Furthermore, simulation data was evaluated for local inhomogeneities (e.g. hot spots or rich mixture pockets). Thus 3D-CFD simulations including gas exchange and injection were carried out for all investigated engine speeds and three EGR rates (0%, 10% and 20%). The intake temperature was set at 35 °C for the speeds 1500 and 2500 1/min and 45 °C for 4000 1/min.

For an EGR rate variation at constant speed it was found that the end of compression temperature is rising with increased EGR rate. At first glance an opposite trend is expected since the three-atomic gases of the exhaust gas have a higher heat capacity than air. However, the heat capacity of the fuel is much higher and since the dilution with EGR reduces the fuel mass fraction the effect of the EGR is overpowered and a slight decrease of the heat capacity is observed, Fig. 13. However, during combustion

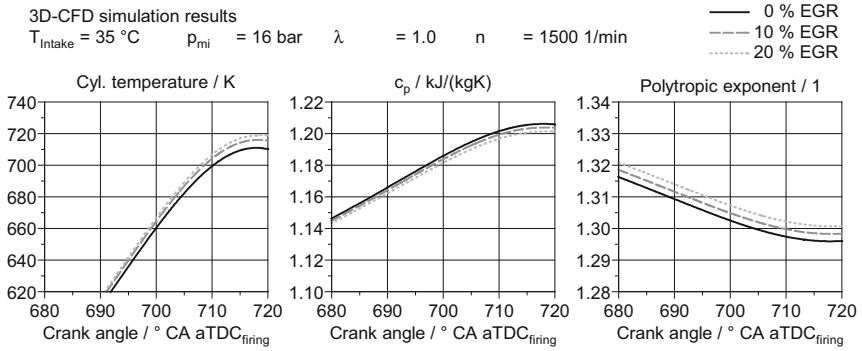


Fig. 13. Impact of EGR on the end of compression temperature at 1500 1/min

the unburned zone is compressed nearly adiabatically and the higher pressures for cases with EGR lead to a reduced temperature increase in the unburned zone [Höp12].

In a next step the stratification at TDC position was analyzed. The simulation results were classified for the quantities residual gas mass fraction (RGF), temperature and rel. AFR. The RGF is distributed very homogeneously since an ideal mix of air and EGR is introduced into the induction system and the high level of charge motion leads to a good mixing with the internal EGR. Small inhomogeneities were found for the rel. AFR in the range of ± 0.15 . For the temperature it was found that usually hot spots with approximately 15 K higher temperature than the bulk gas temperature exist. With the help of the simulation results these hot spots were found to be close to the hot exhaust valves. The effect was strongest when a relatively rich zone is located at one exhaust valve. Due to the less evaporation cooling of the fuel the mixture is found to have the highest temperature in the combustion chamber.

4.2 Combustion Simulation

To analyze the effect of EGR on engine knock, combustion simulations have been carried out. Instead of a conventional combustion model the reduced reaction mechanism from Sect. 2.3 was directly coupled into the CFD simulation. To reduce the numeric effort a multi-zone approach was used. Cells with similar temperature and reaction progress are combined in one chemical reactor [Bap05]. The combustion is initiated with an energy source between the spark plug electrodes and the energy input is set to be half to energy of the primary circuit of the ignition system (45 mJ). For the simulations the KPP value can be derived in the same manner as at the test bench with the help of virtual pressure transducers. Thus the simulation results can be directly compared with the test bench results. For the experimental results cycle-to-cycle variations are observed, which cannot be resolved with the Reynolds-averaged Navier-Stokes (RANS) approach. In order to mimic the test bench behavior spark timing variations in the 3D-CFD simulation were performed to simulate cycles with early, intermediate and late center of combustion.

In Fig. 14 the simulation results at 2500 1/min are depicted. In total five spark timings were simulated for the 0% EGR case of which the last two are within the area of the experimental results. Further advanced spark timings were simulated to verify if the simulation correctly catches the trend of increasing knocking peak to peak values. As shown in the bottom left hand side of Fig. 14 KPP is increasing as expected when the combustion is advanced. The simulation approach is able to correctly reproduce the combustion and knocking behavior at this operating point.

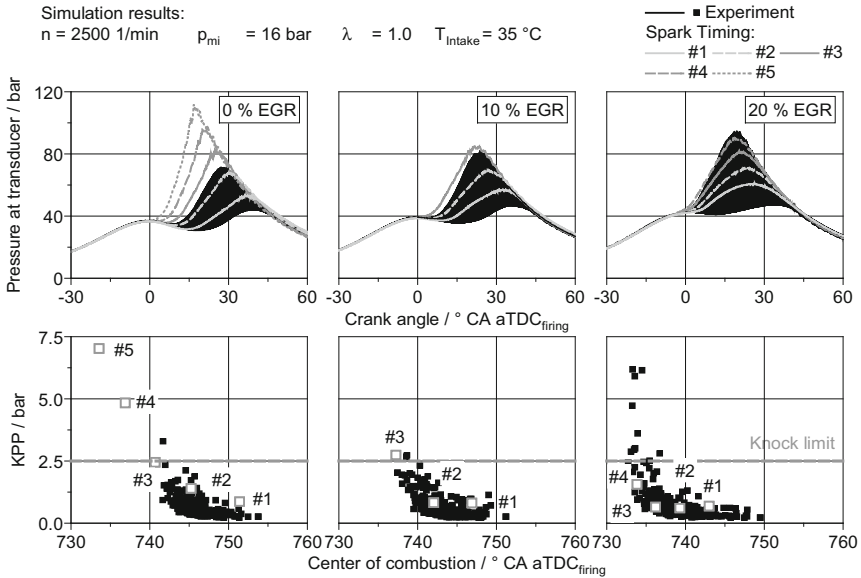


Fig. 14. Comparison of experimental and simulation results at 2500 1/min 16 bar p_{mi}

Figure 14 depicts the results of the EGR variation as well. At 10% EGR the combustion and the knock tendency is accurately reproduced by the simulation results. At 20% the earliest combustion is showing less KPP than measured at the test bench. The higher cycle-to-cycle variations at this operating point make it more difficult to reproduce the knock limit with a RANS approach. However, a similar trend is observed.

In a next step the thermodynamic state of the end gas was analyzed in detail for the different EGR rates. Monitoring positions at a distance of 2.5 mm from the liner surface were set up. During the combustion process the local temperature in the end-gas is increasing by approximately 100 K before the gas at the monitoring positions is consumed by the flame, Fig. 15. When evaluating the local pressure at the time of the first temperature increase no pressure oscillations are observed. Thus this first energy release is not directly connected with the occurrence of knock. The simulation results show that first stage ignition is playing an important role for the relevant

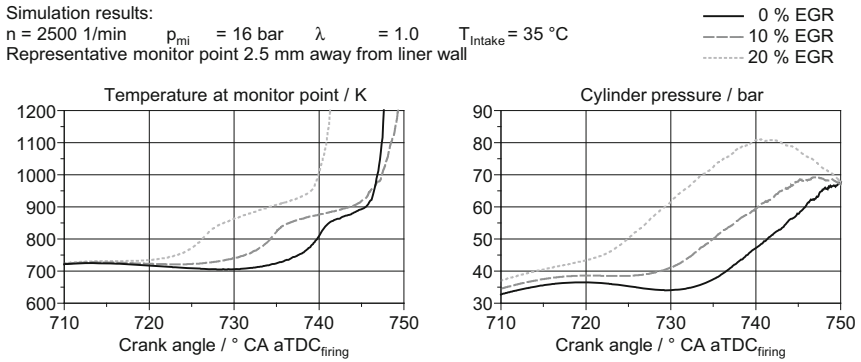


Fig. 15. Representative temperature and pressure in the end-gas zone at 2500 1/min

temperature for engine knock. In all investigated cases the whole end-gas is showing first stage ignition at relatively low mass fraction burned ($x_b < 0.5$).

With increased EGR rate first stage ignition is observed at earlier timings. To understand this behavior constant volume reactor simulations under the influence of EGR were carried out, Fig. 16. The main effect of EGR on the ignition delay time is visible in the prolonged time for the 2nd stage ignition, while first stage ignition is occurring at a similar time. Increasing pressure with EGR leads to similar timings of first stage ignition for simulation with and without EGR. Thus the effect of the first stage ignition is more pronounced with the application of EGR. It can be concluded that considering the first stage ignition is of major importance for the knock modelling (Sect. 5) to correctly predict the occurrence of knock with EGR.

The advantage of using CFD is that the underlying mechanisms of engine knock can be analyzed in a very detailed way. In Fig. 17 the pressure fluctuations for the 0% EGR case with spark timing #5 of Fig. 14 during occurrence of knock are depicted. At 736° CA, a steep pressure rise at the intake side of the combustion chamber is observed. Subsequently, a pressure wave is formed, which travels through the combustion chamber. At 737.2° CA the pressure wave is then reflected at the opposite side

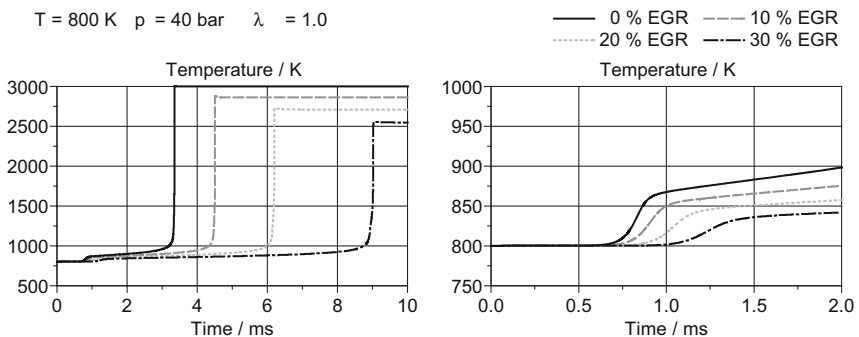


Fig. 16. Temperature trace of auto-ignition under the influence of EGR

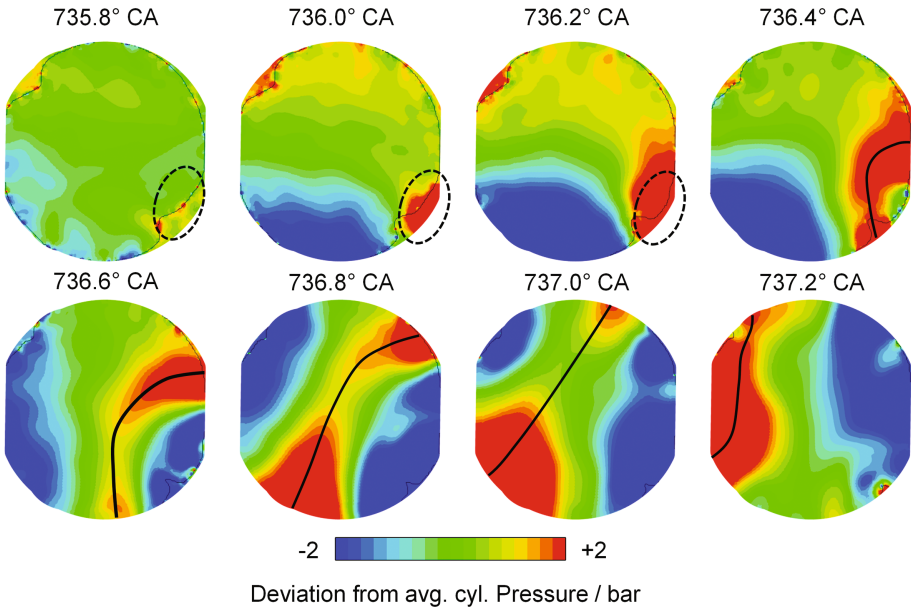


Fig. 17. Visualization of pressure fluctuations during knocking combustion at 2500 1/min, 16 bar p_{mi} and 0% EGR

of the combustion chamber. Finally, a standing wave is created, which leads to the typical pressure oscillations in the simulated pressure at the transducer location.

The coupling of the kinetic mechanism with the CFD model allows analyzing the species concentrations during the occurrence of knock. In Fig. 18 the concentrations of formaldehyde (CH_2O) and hydrogen peroxide (HOOH) are shown for the same operating point. Formaldehyde is a tracer of low temperature combustion and is formed

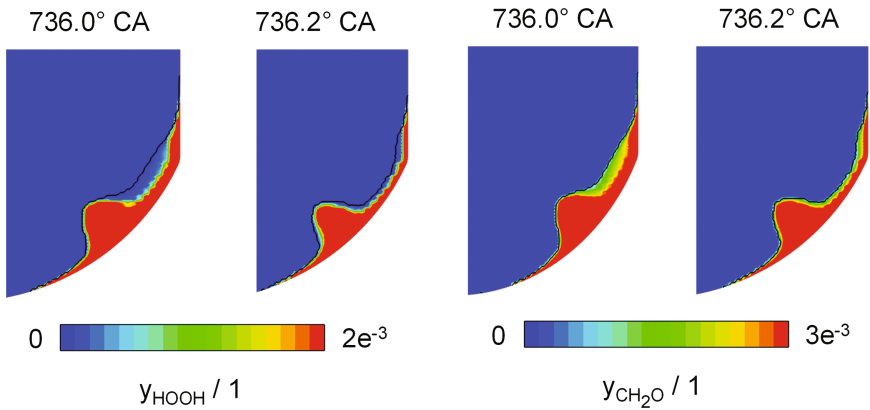


Fig. 18. Consumption of HOOH and CH_2O during the occurrence of knock

during the first stage ignition of the unburned mixture. The flame front is indicated by the black line. At 736° CA the concentration of HOOH ahead of the flame front is decreasing and two OH radicals are formed by the corresponding chemical reaction. Due to the increase in radical concentration CH₂O is consumed and the second stage of ignition is taking place. The fast heat release leads to an increase in temperature and a pressure wave is triggered. With these findings of the 3D-CFD simulations it can be concluded that the new knock model must be capable of predicting both stages of the auto-ignition correctly.

5 Knock Model Development

5.1 General Engine Knock Modeling Approach

The 0D/1D knock models that have been developed in the past 50 years are generally based on the evaluation of an integral representing the pre-reaction state of the unburnt mixture (also known as knock, pre-reaction state and Livengood-Wu integral). Livengood and Wu originally formulated this correlation in 1955 [Liv55]. They proved that the ignition delay time of an air-fuel mixture in motored and firing SI engines can be estimated by evaluating an integral representing the degree of chemical reaction progress and thus the pre-reaction state of the mixture, Eq. (4). Hence, it is possible to predict when auto-ignition of a mixture in an engine will occur (end of integration t_e), if the ignition delay times τ are known at every integration step. These can be measured in a RCM or a shock tube, Sect. 2.1.

$$1 = \int_{t=0}^{t=t_e} \frac{1}{\tau} dt \quad (4)$$

$$\tau \approx C \cdot p^{C_1} \cdot e^{C_2/T} \quad (5)$$

Subsequently, an Arrhenius-type correlation, Eq. (5), can be calibrated by estimating the empirical constants C , C_1 and C_2 and then used for their calculation. The integration process performed in Eq. (4) represents the process of concentration of chain carriers building up, until a pre-defined critical concentration has been reached and exceeded, resulting in an auto-ignition of the air-fuel mixture. The value of the pre-defined critical concentration is constant and thus independent of changes in the boundary conditions, such as e.g. an engine speed increase. Knock modeling approaches commonly used in the 0D/1D engine simulation today are all based on the correlation in Eq. (4). They evaluate the change in the pre-reaction state I_k of an air-fuel mixture between inlet valve close (IVC)/90°CA before Firing Top Dead Center (FTDC) and knock onset (KO) or a constant Mass-Fraction-Burnt-point (usually between MFB75 and MFB85) respectively, as shown in Eq. (6) [Fra91].

$$I_k = \frac{1}{n} \cdot \frac{1}{C} \int_{\alpha=\alpha_{IVC}/90^\circ CA}^{\alpha=\alpha_{KO}/const.MFB} \frac{1}{\tau} d\alpha \quad (6)$$

As soon as the pre-reaction state calculated in Eq. (6) exceeds a constant pre-defined value, the so-called critical pre-reaction state $I_{k,crit}$, knock onset has been reached. The $I_{k,crit}$ value at knock onset corresponds to the critical concentration of chain carriers in the original Livengood-Wu correlation that results in auto-ignition. Hence, the only difference between Eqs. (4) and (6) is the integration domain. Again, the ignition delay times needed for the integration process can be calculated with Eq. (5), after the empirical constants have been estimated. This is commonly done by fitting to measurement data, so that the critical pre-reaction state $I_{k,crit}$ is reached at the measured knock onset. Generally, the mean values of the unburnt zone's parameters estimated with an appropriate two-zone SI combustion modeling approach, e.g. the Entrainment model [Gri06], are used as knock model inputs.

Many different variations of the commonly used knock approach in Eq. (6) have been developed based on measurement data. By adding corresponding terms to Eq. (5), they consider the influence of various boundary conditions on the ignition delay of the air-fuel mixture, such as the AFR and exhaust gas fraction. Alternatively, detailed kinetic reaction mechanisms can be used to calculate the ignition delay times of air-fuel mixtures at various boundary conditions and hence to estimate the values of the empirical constants and to expand Eq. (5). This method has the main advantage of being able to cover a much wider range of boundary conditions than a parameter estimation performed with measurement data from a test bench. Furthermore, the use of detailed mechanisms ensures that no engine-specific effects affect the calculated values. For these reasons, the ignition delay times integrated in the new knock model were estimated with the mechanism developed in Sect. 2.3. However, detailed kinetic reaction mechanisms cannot be integrated in 0D/1D simulations, as this would have a significant negative impact on the typically short computational times. Hence, suitable models for the ignition delay times have to be developed, Sect. 5.4.

5.2 Modeling Approach Performance Investigation

Firstly, the performance of the commonly used knock modeling approach was evaluated by estimating the pre-reaction state of the unburnt mixture of measured knocking single cycles at knock onset. To this end, the knock onset of each knocking cycle, Sect. 3.1, was detected as the location of the minimum of the third derivative of the filtered cylinder pressure. 200 000 single cycles were evaluated in total. In order to obtain the data needed for the performance evaluation, Pressure Trace Analysis (PTA) of the single working cycles was performed. These calculations yield the mean temperature of the unburnt mixture. Subsequently, the pre-reaction state of the unburnt mixture at the measured knock onsets was obtained, Fig. 19. The ignition delay times at each integration step were estimated with a three-domain modeling approach presented in Sect. 5.4.

By neglecting the time span between auto-ignition and the occurrence of oscillations in the measured cylinder pressure resulting from knock (or assuming that it does not change significantly with the operating conditions), it can be concluded that the measured knock onset is also the time of auto-ignition in the unburnt mixture. As discussed in Sect. 5.1, this assumption implies that the calculated pre-reaction states at knock onset have to be equal to the critical pre-reaction state for the investigated engine

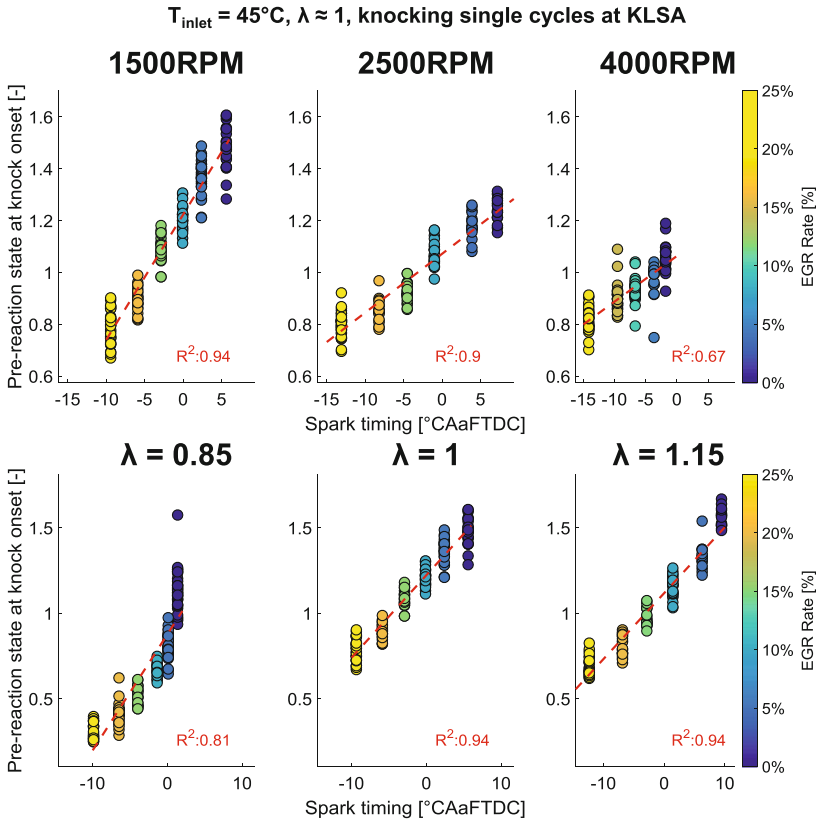


Fig. 19. Pre-reaction state of the unburnt mixture and heat release at measured knock onset of knocking single working cycles at various boundary conditions.

and hence all of the same magnitude. However, Fig. 19 clearly shows significant changes of the values over all investigated operating condition variations. Hence, the knock integral is not capable of accurately estimating the progress of the chemical reactions leading to auto-ignition at in-cylinder conditions, resulting in poor knock prediction performance.

Furthermore, the evaluation of the knock integral is generally performed to an always constant MFB-point, as it is assumed that auto-ignition after this point does not result in knock because of the small unburnt mass and volume fractions left. However, the measured MFB at knock onset changes significantly with the boundary conditions, Fig. 20. Hence, the assumed constant end-of-integration point will also result in a prediction error. Overall, this performance investigation clearly shows that neither the measured knock onset nor the knock boundary can be reliably predicted with the commonly used knock integral, Eq. (6).

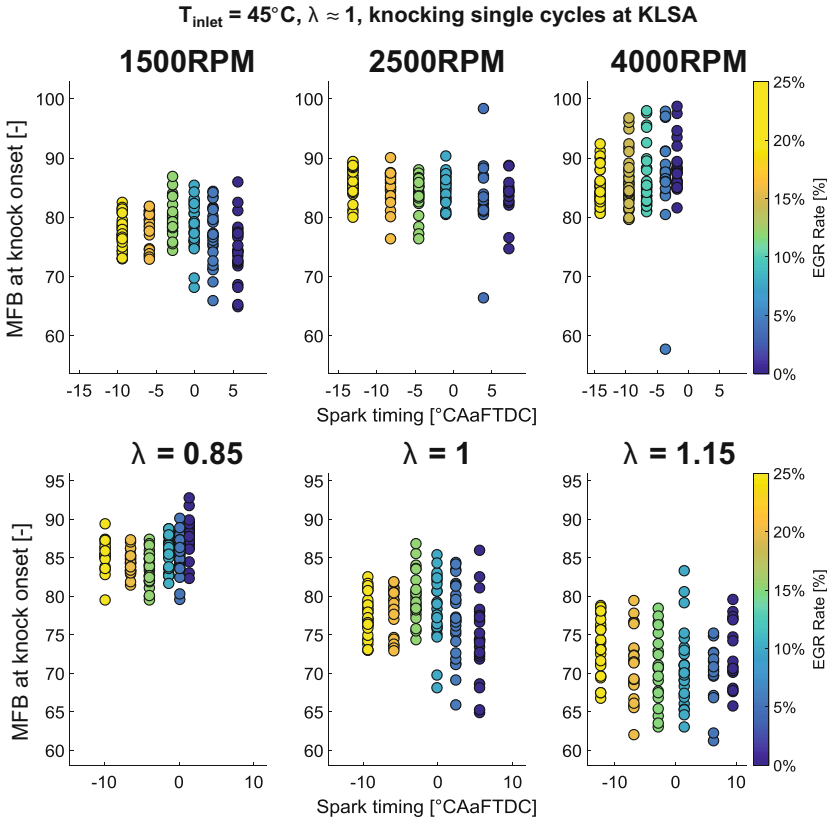


Fig. 20. Mass fraction burnt at measured knock onset of knocking single cycles at various operating conditions.

5.3 In-Cylinder Reaction Kinetic Simulations

In order to better understand the in-cylinder chemical processes resulting in auto-ignition and to investigate the performance of the commonly used simplified chemistry approach – the knock integral – a simulation model representing the unburnt zone of the Entrainment model [Gri06] (or a small spot in it, as the model is scalable) was developed and implemented in Matlab/Cantera. The simulations were performed with the detailed mechanism and the proposed surrogate composition from Sect. 2.

Simulation model

The developed simulation model is based on an adiabatic reactor containing the surrogate-air-exhaust gas mass, Fig. 21. In addition, a moving wall was installed to compress and expand the mixture and hence reproduce the piston movement. Furthermore, the wall has heat transport properties that were used to recreate the wall heat losses calculated by the corresponding model as part of the performed PTA, Sect. 5.2.

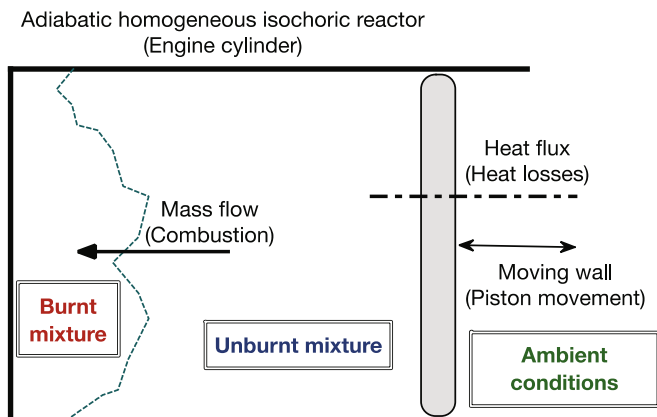


Fig. 21. Model for reaction kinetic simulations at in-cylinder conditions.

As a mass flow from the unburnt into the burnt zone is used in the Entrainment model to represent the combustion [Gri06], the same technique was chosen for this simulation model. Blow-by was considered by evaluating the mass flow rate through an orifice resulting from a pressure gradient. The exhaust gas composition can be calculated from the surrogate component fractions and the AFR by assuming post-catalyst extraction and perfect catalytic conversion. Thus, the initial conditions needed at simulation start are the mixture composition (surrogate, AFR and EGR) as well as the initial volume (piston position), pressure and temperature. The simulations yield if the mixture auto-ignites and when as well as the production and consumption of species causing changes in temperature and pressure. The model was validated by comparing simulated temperature profiles with PTA results in the compression stroke, where no heat release takes place. The curves showed very good agreement.

Investigation findings

By simulating thousands of measured single cycles at various boundary conditions, it was found out that the local auto-ignition in the unburnt mixture resulting in knock can occur in two stages. This phenomenon has already been observed in various studies in the context of gasoline Homogeneous Charge Compression Ignition (gHCCI) [Tan03], but has not been extensively investigated in the context of engine knock. The temperature profiles in Fig. 22 illustrate the two-stage ignition behavior. Obviously, the amount of heat released during the low-temperature ignition depends on the boundary conditions, e.g. engine speed and EGR rate as shown in this case. Generally, two-stage ignition behavior characterizes iso-octane and n-heptane [Tan03]. As these two hydrocarbons, together with toluene and ethanol, compose the surrogate fuel, they also cause the observed low-temperature heat release. The phenomenon is related to the negative temperature coefficient (NTC) zone clearly visible in Fig. 23, where the rate and extent of the hydrocarbon oxidation reactions, which at first increase rapidly with temperature, begin to fall with further rise in the temperature, causing an increase in the ignition delay times in this temperature region. The resulting temperature increase

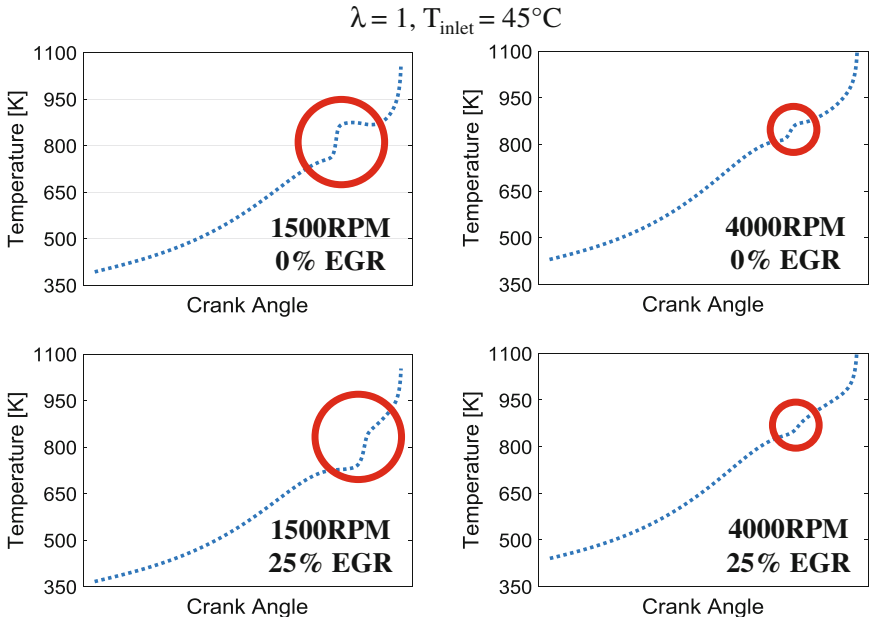


Fig. 22. Simulated temperature profiles of different working cycles with auto-ignition in two stages depending on the boundary conditions.

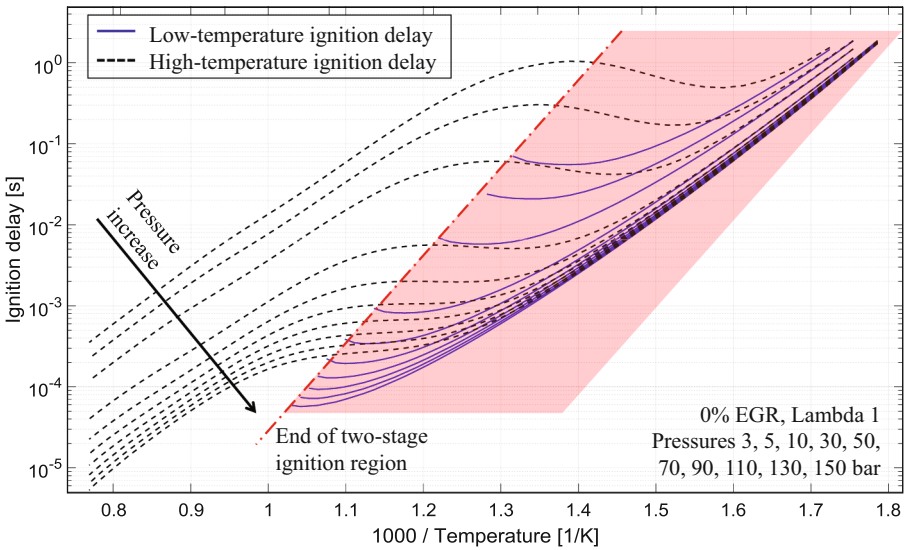


Fig. 23. Two-stage ignition region and ignition delay times of the low- and high-temperature ignition regimes (surrogate from Sect. 2).

influences the following chemical reactions and thus the ignition delay of the mixture significantly [Tan03].

The boundary condition region where two-stage ignition of the surrogate-air mixture occurs is illustrated in Fig. 23. The existence of an ignition delay time of the low-temperature ignition primarily depends on temperature and pressure and defines the two-stage ignition region of a given surrogate composition. Furthermore, Fig. 23 clearly shows that, at high temperatures, the two-stage ignition phenomenon does not occur at all. This observation is relevant for both knock and gHCCI operation with high internal EGR rates, as these lead to high unburnt temperatures.

Knock integral auto-ignition prediction performance

Because of the significant influence of the low-temperature heat release on the mixture's auto-ignition behavior, the question arises, if the commonly used knock integral can consider this effect and thus predict the auto-ignition accurately in case the mixture ignites in two-stages. Figure 24 shows a comparison between the crank angles of auto-ignition simulated with the detailed mechanism with the model presented in Sect. 5.3 and those predicted by a knock integral, Eq. (6), at various boundary conditions. As in Sect. 5.2, the ignition delay times used as integral inputs were obtained with the three-domain modeling approach presented in Sect. 5.4.

Obviously, the occurrence of two-stage ignition results in partially huge errors and hence poor performance of the auto-ignition prediction. For some cycles, no auto-ignition was predicted at all, although the detailed mechanism auto-ignited. Hence, the knock integral cannot account for the low-temperature ignition and its influence on the mixture's ignition delay. These results clearly show that the theoretical approach used for modeling knock in 0D/1D SI engine simulations is not capable of reproducing the in-cylinder behavior of the detailed reaction kinetics mechanism (and thus the "real chemistry"). Thus, it cannot be used for the reliable knock onset prediction in SI engines running on fuels with two-stage auto-ignition behavior, e.g. gasoline. The general knock modeling approach rather has to be changed or improved, in order to consider the occurrence of two-stage ignition.

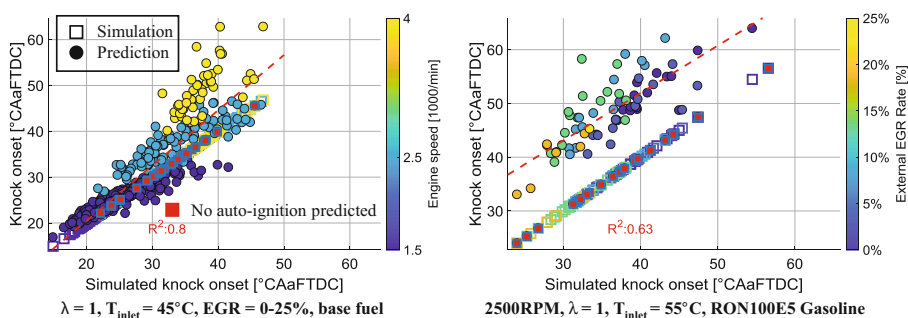


Fig. 24. Times of auto-ignition simulated with the detailed mechanism and predicted by a knock integral at various boundary conditions. For some working cycles, the knock integral predicted no auto-ignition at all.

5.4 Two-Stage Ignition Modeling

An approach for modeling knock that accounts for a low-temperature ignition possibly taking place requires the development of suitable models for the three main parameters characterizing the two-stage ignition phenomenon. These are the ignition delay times of both ignition stages as well as the temperature increase resulting from the low-temperature ignition. First, the quantification of these three parameters is necessary. To this end, following definitions are introduced (Fig. 25):

- The location of the low-temperature ignition τ_{low} is defined as the point $max(T_{grad})$, where the temperature gradient reaches its maximum before the auto-ignition of the mixture.
- The high-temperature or the auto-ignition delay τ_{high} is detected based on a threshold for the temperature gradient; the value was set to 25 K/microsecond.
- The temperature increase T_{incr} resulting from the low-temperature ignition is defined as temperature at simulation start subtracted from the temperature at the point $min(T_{grad})$, where the temperature gradient reaches its minimum between the two ignition stages.

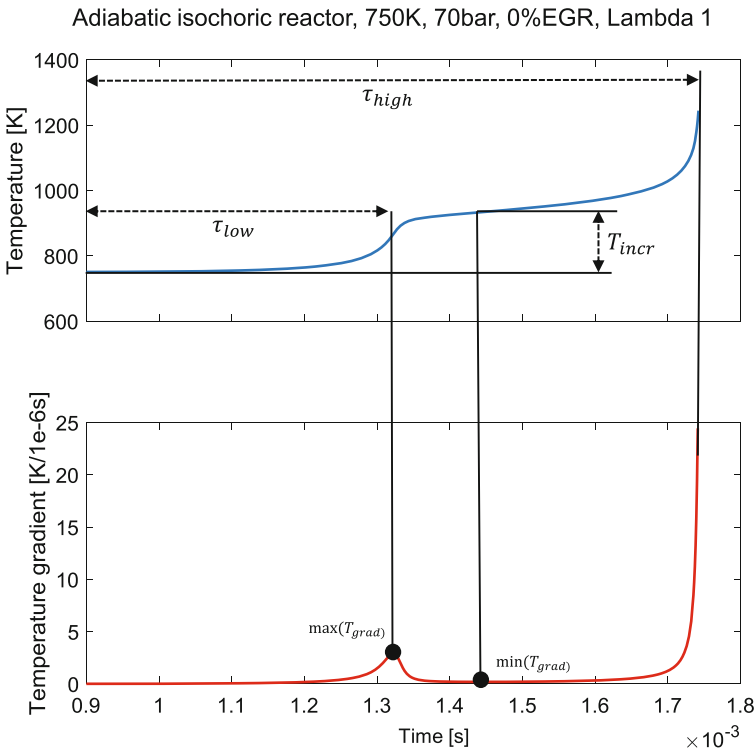


Fig. 25. Definition of low- and high-temperature ignition as well as the temperature increase resulting from the first ignition stage in an adiabatic isochoric reactor at 750 K, 70 bar and $\lambda = 1$, no exhaust gas mass.

The values of the parameters characterizing the two-stage ignition phenomenon were obtained in Cantera/Matlab simulations of an isochoric adiabatic homogeneous reactor with the detailed mechanism already brought up in Sect. 2. An algorithm based on the production of OH radicals followed by their consumption and consequentially temperature increase before the mixture's auto-ignition detected the occurrence of two-stage ignition. The simulated boundary conditions (temperature, pressure, AFR, EGR, ethanol content) were varied according to in-cylinder values typical for SI engines today with the main goal being to cover a sensible value range as wide as possible. Obviously, the exhaust gas composition has to be changed in accordance with the AFR, Sect. 5.3. Moreover, the fractions of the three base surrogate components were varied too, in order to capture the influence of the fuel characteristics on the ignition delay.

The simulation data were used to develop new models for the calculation of the three main parameters characterizing the two-stage ignition phenomenon, with the two main goals being the achievement of high accuracy of the calculated values and short computational times. Clearly, the NTC zone has to be modeled as precisely as possible because of its significant influence on the ignition delay times, Sect. 5.3. The developed models can afterwards be installed in a new knock modeling approach that accounts for the possible occurrence of two-stage ignition and its influence on the mixture's ignition delay. All estimated model parameters should only be recalibrated if values of the parameters characterizing the two-stage ignition phenomenon obtained with a reaction kinetics mechanism different than the one used in this work have to be considered. Further details on the models and their development can be found in [Fan17]; for the sake of completeness, here the model equations are included. The high-temperature ignition delay can be expressed as shown in Eq. (7). This correlation is particularly suitable for fuels with pronounced NTC behavior. Each of the three timescales $\tau_{i,high}$ can be evaluated using a single Arrhenius-type correlation, Eq. (8). Here, the influences of various changes in the boundary conditions are assembled in just two parameters $A_{i,high}$ and $B_{i,high}$. Thus, changes in the boundary conditions are reflected in different values of the activation energy of the chemical reactions leading to auto-ignition (as it is proportional to $B_{i,high}$) [Fan17]. This yields a simple, flexible and yet very powerful modeling approach.

$$\frac{1}{\tau_{high}} = \frac{1}{\tau_{1,high} + \tau_{2,high}} + \frac{1}{\tau_{3,high}} \quad (7)$$

$$\tau_{i,high} = A_{i,high} \cdot e^{\left(\frac{B_{i,high}}{T}\right)}, A_{i,high}, B_{i,high} = f(p, \lambda, EGR, fuel) \quad (8)$$

For the low-temperature ignition delay τ_{low} , it is convenient to choose a modeling approach similar to the one for the auto-ignition delay times, Eqs. (9) and (10). Finally, for the temperature increase resulting from the first ignition stage, the fitted parameter $T_{incr,fit}$ is the sum of the temperature increase T_{incr} and the temperature T_{low} , at which the low-temperature heat release occurred, Eqs. (11) and (12).

$$\frac{1}{\tau_{low}} = \frac{1}{\tau_{1,low} + \tau_{2,low}} \tag{9}$$

$$\tau_{i,low} = A_{i,low} \cdot e^{\left(\frac{B_{i,low}}{T}\right)}, A_{i,low}, B_{i,low} = f(p, \lambda, EGR, fuel) \tag{10}$$

$$T_{incr} = T_{incr,fit} \cdot 100 - T_{low} \tag{11}$$

$$T_{incr,fit} = C_1 \left(\frac{T_{low}}{100}\right)^4 + C_2 \left(\frac{T_{low}}{100}\right)^3 + C_3 \left(\frac{T_{low}}{100}\right)^2 + C_4 \left(\frac{T_{low}}{100}\right)^1 + C_5, \tag{12}$$

$$C_{1..5} = f(p, \lambda, EGR, fuel\ component\ fracs)$$

Additionally, an automatic parameter estimation and optimization of the estimated values was implemented in Matlab to minimize the normalized root mean square deviation of the empirically calculated ignition delay times. Thus, very high model accuracy could be achieved, as shown in Fig. 26 for the high temperature ignition delay. All models account for effects of temperature, pressure, AFR, EGR and the fuel properties (represented by the corresponding surrogate component fractions) [Fan17].

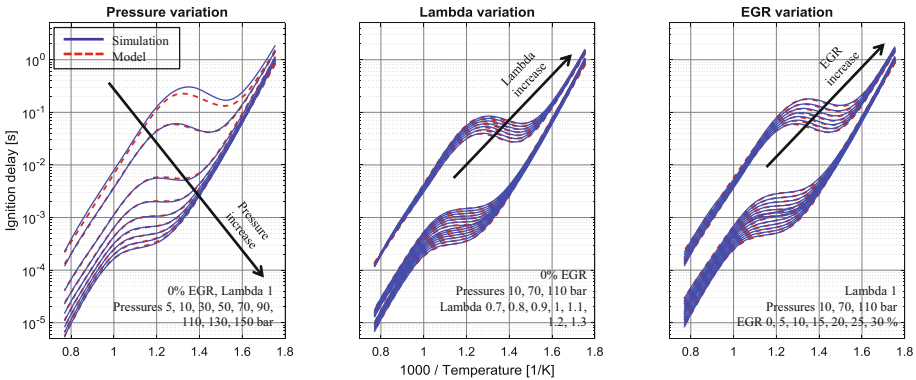


Fig. 26. Simulated and modeled high-temperature ignition delay times at various boundary conditions (surrogate from Sect. 2.2).

5.5 Two-Stage Knock Modeling Approach

The new auto-ignition approach must have the ability to predict the occurrence of two-stage ignition and to consider the significant influence of the low-temperature heat release on the auto-ignition behavior of the mixture, resulting in a reliable prediction of the time of auto-ignition of air-fuel mixtures for fuels with different characteristics at various boundary conditions.

General formulation

The occurrence of each of the ignition events can be predicted by a single knock integral similar to the correlation in Eq. (4), thus yielding a two-stage knock modeling approach, Eq. (13) [Fan17].

$$1 = \int_0^{t_1} \frac{dt}{\tau_{low}(BC)} \xrightarrow[\text{Progress of aggregate reaction}]{\substack{\text{Temperature increase } T_{incr} \\ \text{Pressure increase } p_{incr}}} 1 = \int_{t_1}^{t_2} \frac{dt}{\tau_{high}(BC, T_{incr}(BC), p_{incr}(T_{incr}))} \quad (13)$$

The inputs of the two coupled integrals are the values of the ignition delay for the corresponding ignition stage as a function of the current boundary conditions (denoted by BC in Eq. (13)), calculated by the respective model presented in Sect. 5.4. The estimated time of low-temperature ignition t_l is both upper limit of the first and bottom limit of the second integral. Thus, the integral representing the high-temperature ignition starts as soon as the first integral has reached 1 and the low-temperature ignition has occurred. The resulting temperature increase T_{incr} , as well as the corresponding pressure increase p_{incr} , then have to be added to the respective unburnt mixture values at each integration step of the second integral, Fig. 27. Thus, the influence of the low-temperature ignition on the ignition delay of the mixture is considered. Auto-ignition is defined as the point where the second integral reaches 1, a value that is independent of the boundary conditions representing the constant pre-reaction state of the mixture that has to be reached and exceed for auto-ignition to occur, Sect. 5.1. The integration is performed in the time domain with a small, constant step size of 10^{-7} s.

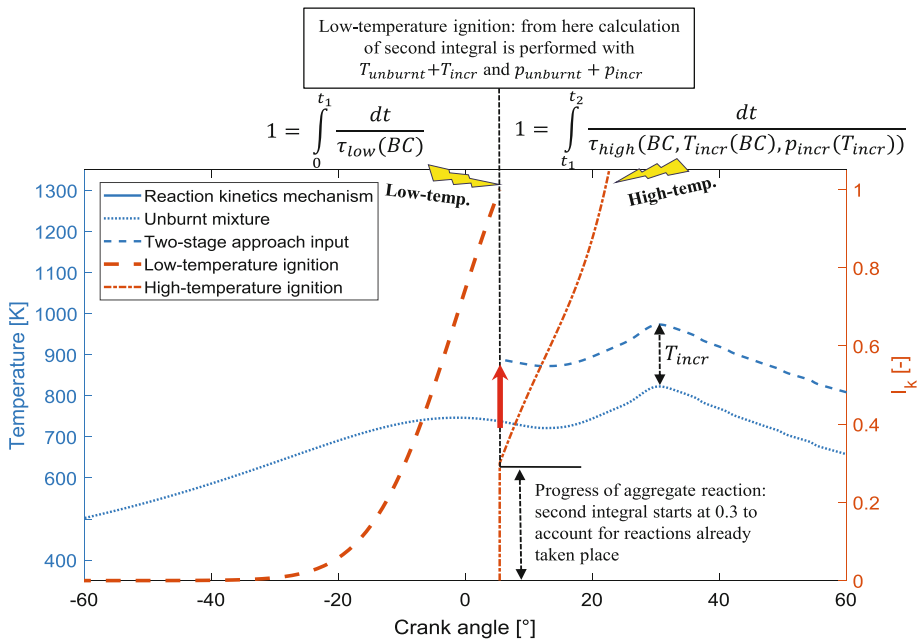


Fig. 27. Auto-ignition prediction for one working cycle considering the occurrence of low-temperature ignition with the newly developed two-stage approach.

Additionally, the progress of the aggregate auto-ignition reaction after the low-temperature ignition has to be considered, as at the starting point of the high-temperature reactions (and the corresponding integral in Eq. (13)), the pre-reaction state is not 0 [Her14]. This is because chemical reactions have already taken place and many intermediate species have been produced, which influences the following reactions significantly. This can also be observed in Fig. 27: the mechanism temperature almost does not change after the first ignition stage, although the cylinder volume is increasing (expansion stroke), thus suggesting that chemical reactions are already taking place and some heat is being released before the auto-ignition. The progress of the aggregate auto-ignition reaction after the first ignition stage was taken into consideration by setting the starting value of the second integral to 0.3, a value independent of the boundary conditions [Fan17].

Thus, the two-stage knock modeling approach involves the calculation of two integrals for the low- and high-temperature ignition respectively, where the second one starts at 0.3 and the temperature and pressure changes caused by the low-temperature ignition are added to the corresponding high-temperature integral inputs. Obviously, for the cycle shown in Fig. 27, the time of auto-ignition could be predicted very accurately, as the locations where the detailed mechanism auto-ignites and the high-temperature ignition integral reaches 1 coincide.

Prediction of two-stage ignition occurrence

The low-temperature ignition integration process in Eq. (13) can only take place as long as a low-temperature ignition delay exists for the respective boundary conditions during integration. This requirement is fulfilled inside the two-stage ignition region shown in Fig. 23. Consequently, if a point outside of this region is reached during the low-temperature ignition integration process (that is still running as the integral has not reached 1), a corresponding low-temperature ignition delay will not be available. Hence, in this case the low-temperature ignition region has been passed through without two-stage ignition occurring. On these terms, the high-temperature integration process in Eq. (13) is directly started at the beginning of the model calculation ($t = 0$) and neither a low-temperature ignition integral nor a temperature increase are considered. Thus, if no two-stage ignition occurs, the common single stage knock integral approach is used. Of course, in this case the ignition delay times are further calculated with the corresponding model proposed in Sect. 5.4.

Approach validation

The new two-stage auto-ignition prediction approach has been extensively validated at various boundary conditions [Fan17]. Validation results comparing the times of auto-ignition (in °CA) simulated with the detailed reaction mechanism at in-cylinder conditions with those estimated with the newly developed two-stage approach can be found in Fig. 28.

Generally, the predicted times of auto-ignition match the corresponding points calculated with the detailed mechanism very good within all boundary condition variations performed. Additionally, the prediction accuracy was validated for 20 different fuels with RONs between 91 and 102 as well as ethanol contents between 0 and 20 vol.%. It is important to remark that neither the critical pre-reaction state (equaling 1), nor the pre-reaction state after the low-temperature ignition (equaling 0.3) were

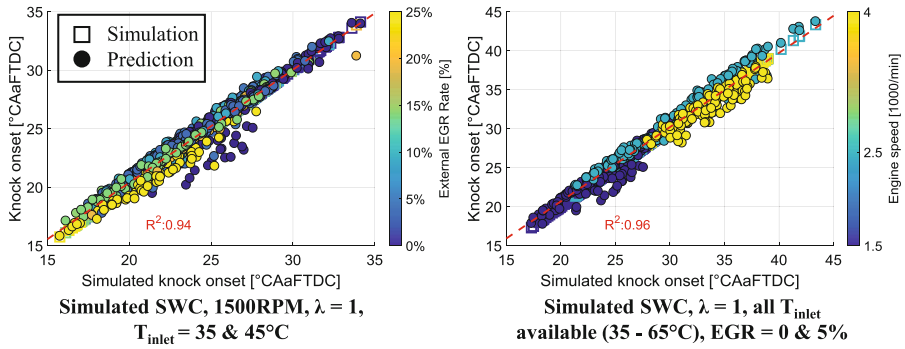


Fig. 28. Times of auto-ignition simulated with the detailed mechanism and predicted by the newly developed two-stage approach at various boundary conditions.

changed within the performed variations of boundary conditions. Hence, the accurate prediction of the time of mixture auto-ignition is ensured, even if the two-stage approach is fully decoupled from the detailed chemistry, and no recalibration of the approach constants is required. Consequently, temperature curves from PTA calculations or OD/ID combustion simulations can be used as knock model inputs, without any recalibration of the auto-ignition model constants. Furthermore, extensive investigations were performed regarding the temperature inhomogeneities (“hot spots”) in the unburnt zone estimated iteratively for measured single cycles and obtained from 3D-CFD stratification analysis, Sect. 4. The results showed that, if the exact values of all knock model inputs are known at each integration step (and not only the mean ones for the unburnt zone), the reliable prediction of knock occurrence based on single and averaged cycles with the two-stage approach is possible without any limitations. Hence, the newly developed modeling approach is generally suitable for the knock boundary prediction in OD/ID engine simulations. The comparison of the auto-ignition prediction performance of the commonly used single integral (Eq. (6)) and the newly

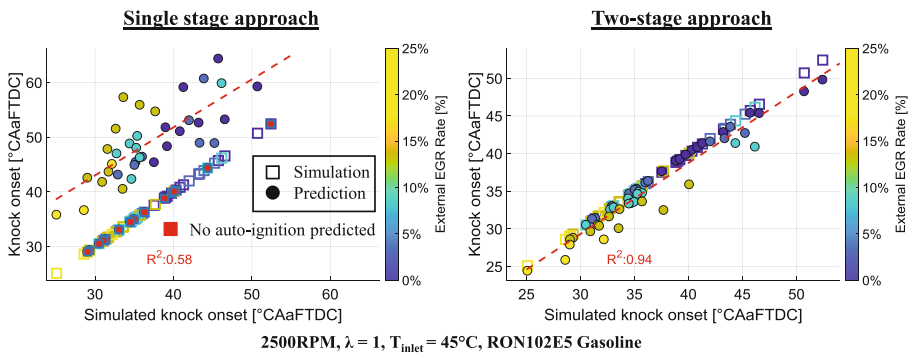


Fig. 29. Auto-ignition prediction with the commonly used single stage and the newly developed two-stage approaches, RON102E5 gasoline. For some working cycles, the single integral predicted no auto-ignition at all.

developed two-stage (Eq. (13)) approaches shown in Fig. 29 makes obvious the huge gain in accuracy achieved in this work. However, a local auto-ignition does not necessarily result in knock [Kön90]. Hence, a criterion for occurrence of knock as a result from the auto-ignition is still needed.

5.6 Knock Occurrence Criterion

As already discussed in Sect. 5.2, a constant end-of-integration point, as assumed in the commonly used knock models, leads to huge prediction errors, because the MFB-point of knock onset changes significantly with the boundary conditions, Fig. 20. Hence, a cycle-individual “latest MFB-point where knock can occur” has to be determined as a function of the boundary conditions. At this point, using an empirical fit will cause problems as soon as the simulated engine configuration or the used simulation models used are changed. Therefore, a knock occurrence criterion based on the unburnt mass fraction in the thermal boundary layer at the time of auto-ignition was developed. This boundary layer develops on the cylinder head, liner and piston over time as a function of a handful of parameters [Lyf84]. As soon as the propagating flame reaches the cylinder walls, the boundary layer at the corresponding locations of contact demolishes. Hence, estimating the unburnt mass fraction in the boundary layer requires spatial information about the flame propagation over time. To this end, a hemispherical flame propagation starting at the spark plug is assumed [Gri06], Fig. 30.

The boundary layer temperature T_{bl} is chosen as the mean value of the unburnt T_u and the wall temperatures [Lyf84]. The layer thickness δ_l at a certain location and a specified point of time can be estimated with Eq. (14) [Lyf84]. The elapsed time t for locations below the FTDC piston position begins at the moment they are uncovered by the piston. For all locations in the clearance volume, FTDC is defined as the starting time.

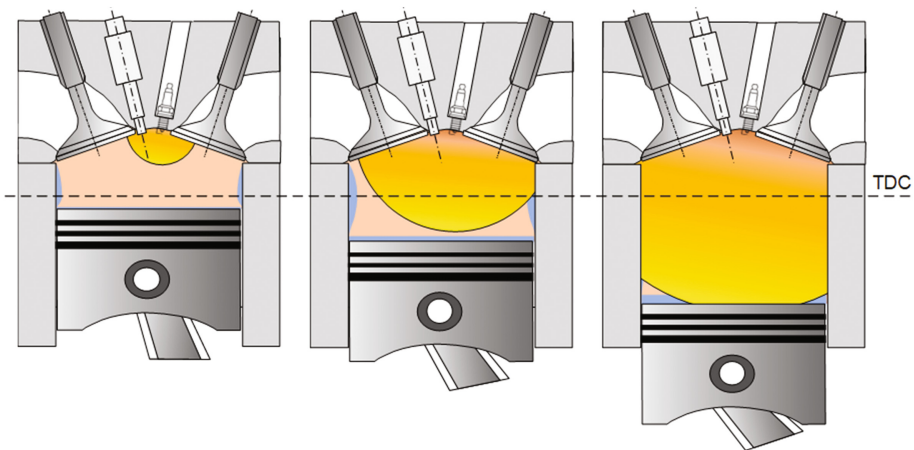


Fig. 30. Exemplary development of the boundary layer on piston and liner over time and counteraction with the flame.

$$\delta_t = 0.6 \cdot Re^{0.2} \cdot \sqrt{\alpha t} \quad (14)$$

$$x_{ub,bl} = \left(\frac{T_{bl}}{T_{ub}} \cdot \left(\frac{1}{V_{ub,bl}} - 1 \right) + 1 \right)^{-1} \quad (15)$$

Equation (14) further involves the calculation of some thermodynamic properties of the gas such as the gas viscosity, thermal conductivity and diffusivity α as well as the Prandtl number. The values of these parameters were evaluated at the boundary layer temperature with the correlations proposed in [Man80]. The local gas velocity needed for the calculation of the Reynolds number Re was evaluated by assuming a one-dimensional axial gas flow with velocity varying linearly from zero at the cylinder head to the piston velocity up at the piston crown [Lyf84]. Consequently, the boundary layer volume $V_{u,bl}$ and thus the fraction of unburnt mass in the boundary layer at a specified point of time $x_{u,bl}$ can be calculated with Eq. (15). The development of the thermal boundary layer is estimated for every working cycle. In this way, the current operating conditions are considered, as they influence the boundary layer development significantly. Hence, the criterion proposed here yields a working cycle individual latest MFB-point where knock can occur. Furthermore, it considers a handful of cylinder parameters, such as the TDC clearance, bore, stroke, spark plug position and the piston diameter. Thus, the knock model also accounts for differences in the engine geometry. A threshold for the unburnt mass fraction at auto-ignition is the only calibration parameter of the knock model and it does not change with the operating conditions. It is assumed that, if the unburnt mass fraction in the boundary layer at auto-ignition is higher than the pre-defined threshold calibrated at the measured knock boundary, no knock can occur. This is because a significant amount of the unburnt mixture has a temperature that equals the one of the boundary layer and hence is much lower than the mean unburnt temperature.

5.7 Short Discussion on the Knock Model Inputs

Because of the mixture and temperature inhomogeneities in the unburnt mass, the question arises, if and how these should be considered. The temperature is by far the most critical knock model input (exponential influence on the ignition delay times of both ignition stages), so small temperature differences can cause significant changes in the auto-ignition behavior predicted by Eq. (13). To this end, extensive investigations were performed to evaluate if temperature and mixture inhomogeneities have to be accounted for in order to reliably predict the knock boundary with the knock onset criterion presented in Sect. 5.6.

Generally, the higher the unburnt temperature level is, the earlier the predicted auto-ignition will occur, and therefore the smaller the unburnt mass fraction in the boundary layer will be at auto-ignition. Thus, inaccuracies in other simulation models or the values of their calibration parameters (e.g. cylinder wall temperatures or wall heat transfer) are reflected in the knock model calibration parameter and can be compensated for by adjusting its value in the course of the model calibration. Consequently, the performed investigations showed that the knock occurrence proposed in

Sect. 5.6 yields accurate prediction results, even if the calculations are performed with the mean unburnt temperature and the global AFR, as will be demonstrated in Sect. 5.8. This can sometimes result in perhaps unrealistic thresholds for the percentage of unburnt mass in the boundary layer at KLSA of about 10–15%, depending on the boundary conditions and the chosen simulation models. However, in this way a sub-model for the mixture and temperature inhomogeneities is not necessarily needed for the reliable prediction of the knock boundary – a fact that eliminates the need for any empirical submodels, as currently no quasi-dimensional inhomogeneities approaches exist. Hence, unlike all commonly used knock models that involve the evaluation of empirical fits containing engine-specific effects, the new model can be applied to different engines without any limitations.

Additional investigations have proven that a similar prediction quality is achievable with different wall heat transfer approaches. Currently, the simulation of single cycles with a respective model does not improve the knock boundary prediction accuracy, as it requires information about the local hot spot temperatures, and leads to a significant increase in computational time. Consequently, the proneness to knock in this case is also assessed based on the respective averaged cycle.

Overall, the flawless model use with different engine configurations is ensured, as no empirical fits derived from measurement data are included in the new knock model. Because of the significant influence of other simulation models on the knock model calibration parameter however, its absolute value is not necessarily meaningful and should not be interpreted.

5.8 Knock Model Validation

The performance of the newly developed knock model has been evaluated extensively at different boundary conditions on three different engines. The validation process involved the comparison of the measured MFB50-points at the knock boundary with the ones predicted by the knock model in the course of 0D/1D engine simulations. For this purpose, all measured operating points were simulated with 0D/1D and three pressure analysis models of the investigated engines. All simulation models (e.g. combustion, turbulence etc.) were calibrated so that they reproduce the behavior of each engine as accurately as possible. Thus, the simulations yield temperature and pressure curves as well as heat release rates similar to those estimated from the test bench data. The single knock model calibration parameter was estimated at one operating point for each of the investigated engines respectively and subsequently kept constant during the validation process.

The main validation goal was to ensure the model responds correctly to changes in the engine configuration and operating conditions represented by the direction of shift of the MFB50-points at the knock boundary. A further objective was to achieve an error in the predicted MFB50-point at the knock boundary of 2°C_A or less with the constant threshold for the unburnt mass fraction in the cool boundary layer, calibrated at the measured knock boundary. Furthermore, because the knock model does not include any empirical submodels that could contain engine-specific effects, it is expected that the quality of knock boundary prediction does not vary significantly

between different engines, provided that the calibration quality of the rest of the simulation models is equal.

Engine 1

To begin with, the knock model performance was evaluated for the single-cylinder engine setup presented in Sect. 3.1, Fig. 31. The operating points include variations of engine speed, EGR rate, inlet temperature and AFR (full load enrichment replacement by EGR). Overall, the prediction performance of the new knock model is very good and the effects of all boundary conditions on the KLSA are predicted correctly. When assessing the prediction performance of the new model, it should be considered that each measured point at the knock boundary has a different knock frequency, as the boundary was defined as a knock frequency window, Sect. 3.1. Nevertheless, the calculated MFB50-points at the knock boundary are within the defined limits of 2°C. This high prediction quality enables the investigation of different combustion systems, engine configurations and operating conditions.

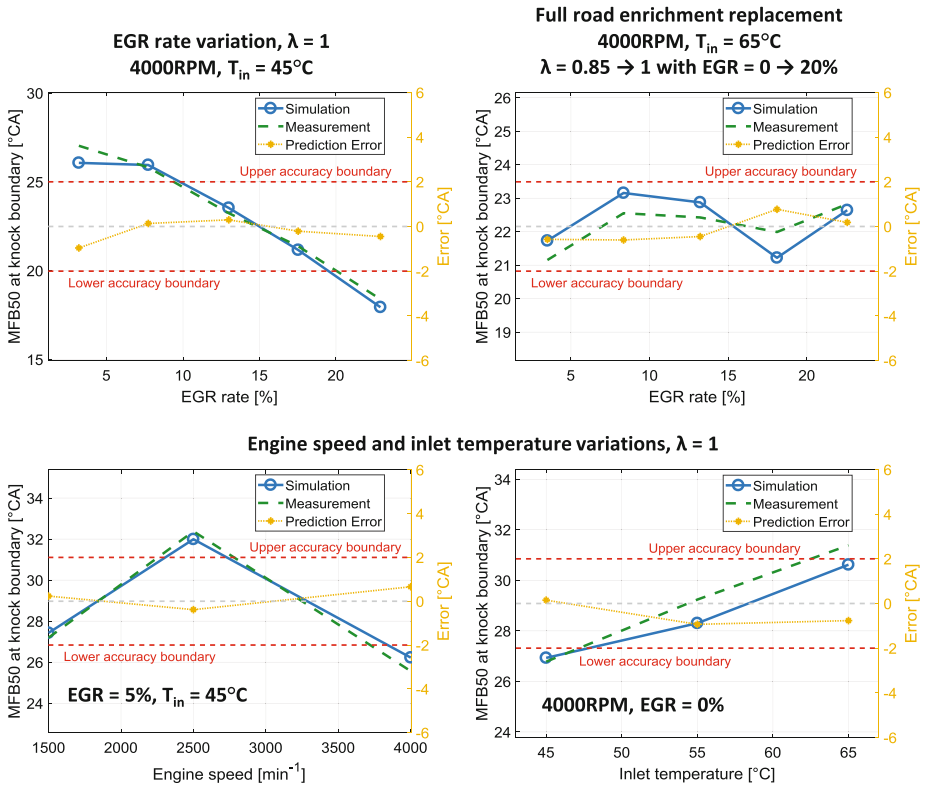


Fig. 31. Knock model validation, engine 1.

Engine 2

The second engine is a single-cylinder configuration that differs significantly from engine 1, as it has a different cylinder head with a tumble runner design and piston with a higher compression ratio of 11.84, Sect. 3.1. The corresponding model validation results for a load increase can be found in Fig. 32. Again, the prediction quality is very high, despite the significant change in the unburnt temperature level with engine load. Hence, the model is capable of reliably predicting the influence of different loads (and thus compression ratios, as this parameter affects the knock model inputs in a similar way) on the knock behavior.

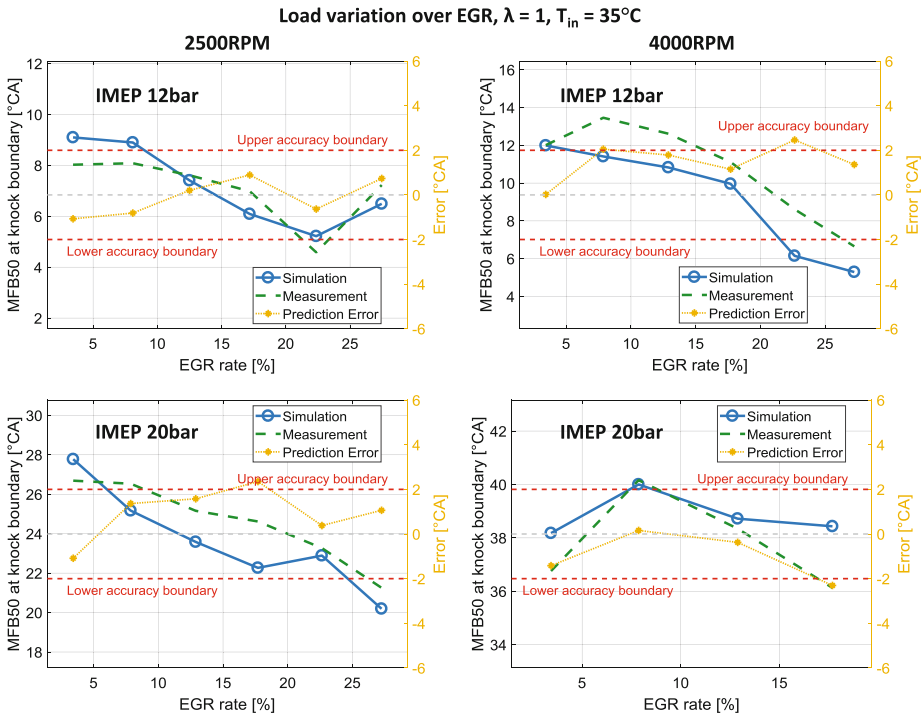


Fig. 32. Knock model validation, engine 2.

Engine 3

The third engine the knock model performance was evaluated on is a three-cylinder configuration described in [Hop15]. Because of the EGR cooler’s limited cooling power, at higher EGR rates, the inlet temperature could not be maintained constant, Fig. 33. This on the other hand led to a decrease in the effective mean pressure at the knock boundary. Hence, this measurement series contains significant simultaneous changes in a handful of the operating conditions at a very high engine speed of 5500RPM. Despite the complex interrelations these result in, the performance of the

knock model is very good, with both the direction of the shift and the absolute values of the MFB50-points at the knock boundary being predicted accurately by the new model, Fig. 33.

Overall, the model validation has shown that the model considers changes in the engine configuration and operating conditions correctly by accurately predicting the direction of the shift of the MFB50-points and their absolute values at the knock boundary. Moreover, the model has been successfully validated on three different engines with no significant variations in the knock boundary prediction quality. It has been demonstrated that an excellent knock prediction performance can be achieved with the mean values of the unburnt mixture’s parameters being used as model inputs, even if the operating conditions change significantly. This is possible thanks to the lack of any empirical submodels, the very accurate two-stage auto-ignition prediction and the cycle-individual knock occurrence criterion that takes cylinder geometry, flame propagation and the operating conditions into account.

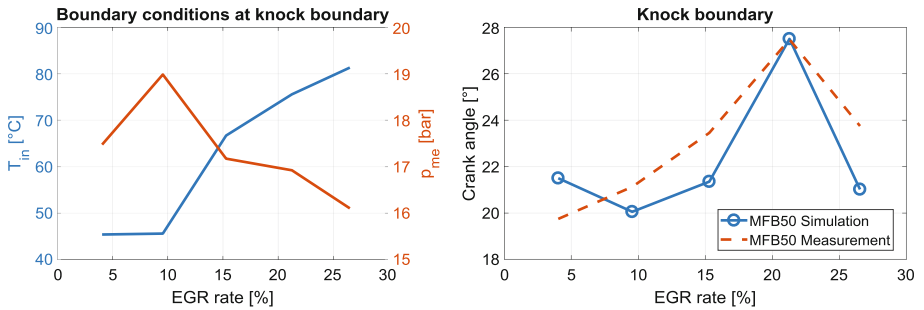


Fig. 33. Knock model validation, engine 3.

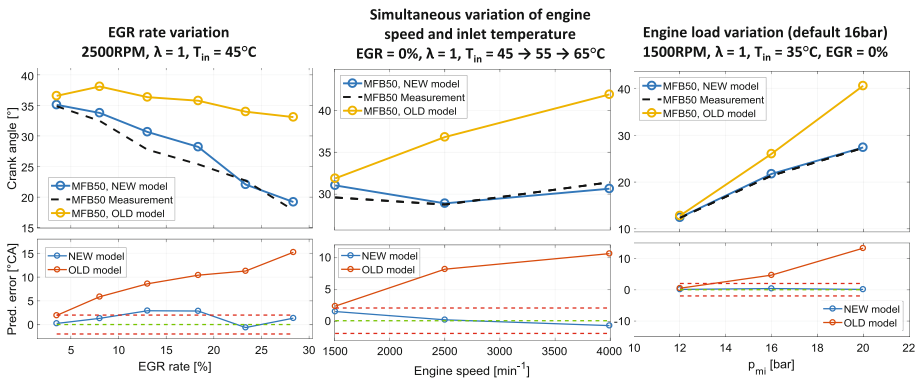


Fig. 34. Knock boundary prediction with a commonly used and the newly developed knock models.

Finally, Fig. 34 shows a comparison between the knock boundaries predicted with the newly developed knock model and an approach commonly used today [Sch10], demonstrating the overall huge gain in prediction accuracy achieved in this work.

6 Conclusion and Outlook

With the help of fundamental investigations the auto-ignition delay times of a gasoline fuel under the presence of EGR were measured. Based on recent research a surrogate mixture has been defined, which was successfully validated in a CFR engine for RON and MON. Subsequently a kinetic mechanism for gasoline surrogate fuels was developed and validated with the measurement data. For application in simulation models this mechanism has been reduced while maintaining a high accuracy. With the help of this mechanism problems involving real gasoline fuels especially in the field of EGR diluted combustion systems can be analyzed in more detail.

Single cylinder experiments were performed to investigate the influence of EGR on combustion in a detailed way. EGR was found to successfully inhibit knock allowing an up to 9° CA advanced center of combustion and an about 4% increased indicated efficiency at an EGR rate of 25%. For the number of knocking cycles, an exponential increase was observed in the area of KLSA. With spark timings relative to the KLSA similar knocking behavior with and without EGR was observed. The influence of nitric oxide on engine knock was studied as well. Trace amounts of NO (100 ppm) were found to lead to stronger knock limitation. With either decreased or increased NO concentration the knock tendency was reduced. With these findings experiments with catalyzed exhaust gas were carried out. Experimental results revealed that post catalyst extraction is favorable when the cylinder NO concentration can be reduced well below 100 ppm allowing a 2° CA advanced center of combustion at 25% EGR.

The kinetic mechanism was used in a new approach to predict the occurrence of knock in 3D-CFD simulations. For the investigated operating points the knock limit of an EGR combustion system could be detected with sufficient accuracy. Detailed analysis of the simulation results showed that two-stage ignition is playing a major role during knock occurrence for EGR combustion systems. A pool of formaldehyde and hydrogen peroxide is formed during first stage ignition which is then consumed during the second stage of ignition. Subsequently a pressure wave is triggered.

By developing a model reproducing the unburnt mixture at in-cylinder conditions and simulating thousands of working cycles with a detailed reaction kinetics mechanism, it was confirmed that two-stage ignition can occur in the unburnt mixture in conventional SI engines, resulting in knock. Subsequently, a two-stage knock integral approach was proposed for the prediction of the time of auto-ignition. Furthermore, a criterion for knock occurring as a result from the auto-ignition based on the unburnt mass fraction in the cool thermal boundary layer was developed. Finally, the excellent prediction performance of the new knock model was demonstrated on three different engines. The newly developed knock model for the 0D/1D SI engine simulation contains no empirical submodels and has just one calibration parameter that does not change with the boundary conditions. Therefore, the new model can be applied to different engines without any limitations, after a simple recalibration.

Acknowledgements. The presented work has been performed as part of the research tasks within the project “Knock with EGR at full load” defined and financed by the Research Association for Combustion Engines (FVV) e.V. (FVV Project 6301). The authors would like to thank the working group that accompanied the research work and all the companies involved for their support as well as the FVV for granting the financing.

Abbreviations

α_{h50}	Center of combustion
λ	Relative air-to-fuel ratio
AFR	Air-to-Fuel Ratio
aTDC	After top dead center
bTDC	Before top dead center
c_p	Specific heat capacity at constant pressure
CA	Crank angle
CFD	Computational fluid dynamics
CH ₂ O	Formaldehyde
CO	Carbon monoxide
CO ₂	Carbon dioxide
D	Diameter/Bore
DI	Direct injection
DOHC	Double overhead camshaft
EGR	Exhaust gas recirculation
gHCCI	Gasoline Homogeneous Charge Compression Ignition
HC	Hydrocarbons
HOOH	Hydrogen peroxide
KLSA	Knock Limited Spark Advance
KO	Knock Onset
KPP	Knock Peak-to-Peak
MFB	Mass Fraction Burned
MON	Motor octane number
n	Engine speed
NO _x	Nitrogen oxides
NTC	Negative Temperature Coefficient
O ₂	Oxygen
p_{mi}	Indicated mean effective pressure
PN	Particulate number
PTA	Pressure Trace Analysis
RANS	Reynolds-averaged Navier-Stokes equations
RCM	Rapid compression machine
RGF	Residual gas mass fraction
RON	Research octane number
s	Stroke
ST	Shocktube
TDC _{firing}	Firing Top Dead Center
x_{EGR}	EGR rate

References

- [Alg07] Alger, T., Gingrich, J., Mangold, B.: The effect of hydrogen enrichment on EGR tolerance in spark ignited engines, SAE Technical Paper 2007-01-0475 (2007)
- [And10] Andersen, V.F., Anderson, J.E., Wallington, T.J., Mueller, S.A., Nielsen, O.J.: Distillation curves for alcohol-gasoline blends. *Energy Fuels* **24**, 2683–2691 (2010)
- [Bap05] Babajimopoulos, A., Assanis, D.N., Flowers, D.L., Aceves, S.M., Hessel, R.P.: A fully integrated computational fluid dynamics and multi-zone model with detailed chemical kinetics for the simulation of premixed charge compression ignition engines. *Int. J. Engine Res.* **6**, 497–512 (2005)
- [Ben76] Benson, S.W.: *Thermochemical Kinetics*, 2nd edn. Wiley, New York (1976)
- [Bur15] Burke, S.M., Simmie, J.M., Curran, H.J.: Critical evaluation of thermochemical properties of C1–C4 species: updated group-contributions to estimate thermochemical properties. *J. Phys. Chem. Ref. Data* **44**, 013101 (2015)
- [Cai16] Cai, L., Pitsch, H.: Optimized chemical mechanism for combustion of gasoline surrogate fuels. *Combust. Flame* **162**, 1623–1637 (2015)
- [Cai16_2] Cai, L., Pitsch, H., Mohamed, S.Y., Raman, V., Bugler, J., Curran, H., Sarathy, S. M.: Optimized reaction mechanism rate rules for ignition of normal alkanes. *Combust. Flame* **173**, 468–482 (2016)
- [Cur02] Curran, H., Gaffuri, P., Pitz, W.J., Westbrook, C.K.: A comprehensive modeling study of iso-octane oxidation. *Combust. Flame* **129**, 253–280 (2002)
- [Deb06] Dubreuil, A., Foucher, F., Mounaïm-Rousselle, C.: Effect of EGR chemical components and intake temperature on HCCI combustion development, SAE Technical Paper 2006-32-0044 (2006)
- [Fan17] Fandakov, A., Grill, M., Bargende, M., Kulzer, A.C.: Two-stage ignition occurrence in the end gas and modeling its influence on engine knock, SAE Technical Paper 2017-24-0001 (2017)
- [Fra91] Franzke, D.: Beitrag zur Ermittlung eines Klopfkriteriums der ottomotorischen Verbrennung und zur Vorausberechnung der Klopfgrenze, Ph.D. thesis, Technical University of Munich (1991)
- [Goo15] Goodwin, D.G.; Moffat, H.K., Speth, R.L.: Cantera: an object-oriented software toolkit for chemical kinetics, thermodynamics, and transport processes, Version 2.2.1, Zenodo (2016)
- [Gri06] Grill, M., Billinger, T., Bargende, M.: Quasi-dimensional modeling of spark ignition engine combustion with variable valve train, SAE Technical Paper 2006-01-1107 (2006)
- [Her14] Hernández, J., Lapuerta, M., Sanz-Argent, J.: Autoignition prediction capability of the Livengood–Wu correlation applied to fuels of commercial interest. *Int. J. Engine Res.* **15**(7), 817–829 (2014)
- [Hop15] Hoppe, P., Lehrheuer, B., Pischinger, S.: Downsizing with Biofuels II, Final Report, FVV Spring Conference, Research Association for Combustion Engines (FVV) e. V., Bad Neuenahr (2015)
- [Höp12] Hoepke, B., Jannsen, S., Kasseris, E., Cheng, W.: EGR effects on boosted SI engine operation and knock integral correlation. *SAE Int. J. Eng.* **5**(2), 547–559 (2012)
- [Jak11] Jakob, M., Pischinger, S., Adomeit, P., Brunn, A., Ewald, J.: Effect of intake port design on the flow field stability of a gasoline DI engine, SAE Technical Paper 2011-01-1284 (2011)
- [Kön90] König, G., Maly, R., Bradley, D., Lau, A., et al.: Role of exothermic centres on knock initiation and knock damage, SAE Technical Paper 902136 (1990)

- [Lee12] Lee, C.S., Vranckx, S., Heufer, K.A., Khomik, S.V., Uygun, Y., Olivier, H., Fernandez, R.X.: On the chemical kinetics of ethanol oxidation: shock tube, rapid compression machine and detailed modeling study. *Z. Phys. Chem.* **226**, 1–28 (2012)
- [Liv55] Livengood, J.C., Wu, P.C.: Correlation of autoignition phenomena in internal combustion engines and rapid compression machines. In: *Symposium International Combustion* (1955)
- [Lyf84] Lyford-Pike, E.J., Heywood, J.B.: Thermal boundary layer thickness in the cylinder of a spark-ignition engine. *Int. J. Heat Mass Transf.* **27**(10), 1873–1878 (1984)
- [Man80] Mansouri, S.H., Heywood, J.B.: Correlations for the viscosity and Prandtl number of hydrocarbon-air combustion products. *Combust. Sci. Technol.* **23**, 251–256 (1980)
- [Mor05] Morley, C.: Gaseq. <http://www.gaseq.co.uk/>
- [Mor10] Morgan, N., Smallbone, A., Bhave, A., Kraft, M., Cracknell, R., Kalghatgi, G.: Mapping surrogate gasoline compositions into RON/MON space. *Combust. Flame* **157**, 1122–1131 (2010)
- [Par15] Parsons, D., Akehurst, S., Brace, C.: The potential of catalysed exhaust gas recirculation to improve high-load operation in spark ignition engine. *Int. J. Eng. Res.* **16**, 592–605 (2015)
- [Pep07] Pepiot-Desjardins, P., Pitsch, H.: An efficient error-propagation-based reduction method for large chemical kinetic mechanisms. *Combust. Flame* **154**, 67–81 (2008)
- [Sch10] Schmid, A., Grill, M., Berner, H.-J., Bargende, M.: A new approach for SI-Knock prediction. In: *3. IAV International Conference on Knocking in Gasoline Engines*, Berlin (2010)
- [She14] Shock and Detonation Toolbox. <http://shepherd.caltech.edu/EDL>
- [Sun14] Sung, C.-J., Curran, H.J.: Using rapid compression machines for chemical kinetics studies. *Progress Energy Combust. Sci.* **44**, 1–18 (2014)
- [Tan03] Tanaka, S., Ayala, F., Keck, J.C., Heywood, J.B.: Two-stage ignition in HCCI combustion and HCCI control by fuels and additives. *Combust. Flame* **132**, 219–239 (2003)
- [Zha16] Zhang, K., Banyon, C., Bugler, J., Curran, H.J., Rodriguez, A., Herbinet, O., Battin-Leclerc, F., B'Chir, C., Heufer, K.A.: An updated experimental and kinetic modeling study of n-heptane oxidation. *Combust. Flame* **172**, 116–135 (2016)